Solid-State Diffusion Bonding Inconel 718 to Itself for Sheet Laminate Additive Manufacturing

by

Preston Regg Angell

A Thesis Presented in Partial Fulfillment
of the Requirements for the Degree
Master of Science

Approved October 2025 by the
Graduate Supervisory Committee:

Leila Ladani, Chair
Jafar Razmi
Yang Jiao

ARIZONA STATE UNIVERSITY

December 2025

ABSTRACT

Transient liquid phase diffusion bonding is a common process used to join stacked laminates for the sheet laminate additive manufacturing process. The joining process implements interlayer materials that contain melting point depressants (MDP) which alleviate some production challenges and aid in the bonding process. While this thin interlayer material assists some of the challenges associated with production, it also introduces new elements into the base material. This contamination can reduce the solidus temperature of the base material and affect subsequent production processes. Solid-state diffusion bonding, without the aid of an interlayer material, can offer similar results to transient liquid phase diffusion bonding without contaminating the base material. However, bonding in the solid-state adds production challenges associated with the laminates' surface finish and the accompanying higher pressure levels required to achieve intimate contact between substrates. Omitting interlayer materials also removes any concentration gradient, which gives the net flux of diffusing atoms direction of flow. Without a concentration gradient, the process must largely rely on the random walk theory.

Iterative experiments were conducted using Inconel alloy 718 substrates bonded in a Centorr vacuum furnace hot press at various super solvus temperatures, pressures, surface roughness, and hold times. All samples were processed with an AMS2774 condition S1750DP heat treatment after the bonding process to precipitation harden the solid-state bonded material. To characterize the results of the experiments, samples were subjected

to metallographic, scanning electron microscope, Vickers microhardness, and room temperature tensile testing.

Results of the experiment show that diffusion bonding alloy 718 at super solvus temperatures without the aid of an interlayer material is possible but results in low yield strength, relative to the base material. This low yield strength is due to large grains as a result of the super solvus diffusion bonding process. Large Niobium rich carbides and Titanium rich nitrides were present throughout all samples and were considerably larger in samples bonded above 1200°C. It is theorized that the large NbC and TiN precipitates could have depleted the bulk of valuable precipitation forming elements, resulting in less precipitation hardening on bonded samples with large precipitates.

ACKNOWLEDGMENTS

This work was in part funded by the National Science Foundation under grant number 2152254, and the Office of Naval Research grant number N000142512218. Honeywell Aerospace Technologies allowed the use of their research hot press vacuum furnace and laboratory equipment to support this research. The author is especially thankful to Lindsay Angell for supporting the research efforts and proofreading the rough draft. Chloe Faust provided significant support performing the grain size measurement calculations and for compiling the large amount of bonding, heat treatment and testing data. John Perek, Camden Brooks, Dr. Mark Carroll, and Brent Widder were great consultation resources that helped troubleshoot issues and give guidance on testing.

TABLE OF CONTENTS

Page

LIST OF TABLES

Table Page

LIST OF FIGURES

INTRODUCTION

Sheet laminate additive manufacturing uses thin, intricately cut sheets stacked on top of one another that are then joined together to create a three-dimensional structure that cannot be produced with traditional manufacturing techniques. Joining is typically completed with ultrasonic welding but can also be completed with brazing, transient liquid phase diffusion bonding, and solid-state diffusion bonding. This process is sometimes advantageous over modern additive manufacturing processes such as Laser Powder Bed Fusion (LPBF) when working with alloys considered to be un-weldable with fusion welding processes, when designs need crisp sharp edges, when internal cooling channels must be microscopic in size, and where partially melted particles would be detrimental to a product [1].

Diffusion bonding is defined as the process of joining materials in solid state to make a monolithic joint at the atomic level [2]. This process is achieved by applying a load to a weldment near a corresponding yielding temperature to locally cause plastic deformation of the joint interface and foster the sharing of atoms between substrates. The bonding is achieved through solid state diffusion of atoms across the joint interface over a time period. High temperatures are applied to increase atomic mobility, diffusion rates and facilitate bonding. This solid-state welding process creates a metallurgical bond making the two materials indistinguishable at a microscopic level. The AWS Welding Handbook listed the process advantages as: extremely high-quality joints, ability to achieve uniform mechanical properties similar to the optimized base material, the ability to join dissimilar metals, and little to no distortion. Some of the process's disadvantages noted were high

tooling and development costs, long processing times, and complex quality assurance processes [3]. A comprehensive study conducted by Garrett, et al. outlines the essential variables of solid-state bonding as: substrate surface finish, process temperature, atmosphere control, applied pressure, and materials weldability. Their broad analysis covered typical process applications and common challenges in the process [4].

Diffusion bonding leverages Fick's laws of diffusion to achieve coalescence by bringing two materials into close contact allowing atoms to be shared between them. Ideally, sharing of atoms between the substrates essentially eliminates the joint interface. For interdiffusion of atoms to occur, the substrate surfaces must come in contact at atomic levels. Even the best surface polishes have oxides as well as microscopic peaks and valleys that prevent large areas from coming into contact.

Diffusion flux is also dependent on the concentration gradient of atoms. As a result of this, diffusion welding often implements interlayer materials which serve the purpose of introducing a strong concentration gradient. Melting point depressants can be added to this interlayer to help achieve intimate contact of faying surfaces by completing the process via Transient Liquid Phase Diffusion Bonding (TLPDB). As a result of this interlayer material, the nominal composition of the material will contain additional alloying elements. This can hypothetically change the composition of the base materials or contaminate the base material near the joint interface, especially when melting point depressants are added to the interlayer material and the weldment is completed via TLPDB. For this reason, this research will explore the feasibility of completing Solid

State Diffusion Welding (SSDBW) without the aid of an interlayer material. Theoretically, this will keep the material's chemical composition pure and will provide desired physical and mechanical properties relative to materials that implement an interlayer material.

CHAPTER 1

HISTORICAL BACKGROUND OF JOINING METALS

1.1 Origins of Joining Metals

Joining metals dates back to ancient times in the middle east (modern-day Iraq and Egypt) which is generally accepted to be ~5000 BC. The typical applications were on jewelry and fine decorative items. The joining process is consistent with what we today know as brazing where a gold or copper braze filler material was used to flow into joints creating a metallurgical bond between the materials. Tombs wall paintings in Egypt portray the use of mouth blowpipes for the brazing process. Brazing processes continued throughout the bronze age and showed increasing levels of sophistication and complexities, some even showing two step processes where brazed components would have more than one assembled component, showing knowledge of different melting temperature alloys [5]. Various brazing processes continue to be used today and are commonly used in the aerospace, automotive, and nuclear applications. Braze filler materials have gotten significantly more sophisticated by implementing melting point depressant alloying elements to the braze filler material giving the ability to more closely match material properties.

1.2 Solid State Welding

Solid State Welding can be traced back to the beginning of the iron age (1200 BC) and is known to be the first form of welding. The process, most commonly used, included heating iron to the point of glowing and then plastically deforming them it into one another by repeated blows of a hammer or press. A metallurgical bond is achieved

ultimately through the diffusion process. This process is recognized in modern times to be forge welding [6]. Forge welding was used in ancient India to create wootz steel (today known as Damascus steel) which layers alternating laminates of steels, varying in composition, folded into each other hundreds of times to create macroscopically alloyed blades and swords. This material was known to be much harder than generic irons that were common at the time and as a result was much better at holding a sharp edge [7]. Today, Damascus steel is used to create materials that are used almost exclusively for their aesthetic appeal rather than for desired mechanical properties. Most common form is to alternate a steel alloy and nickel-based alloys to make a stark contrast which is visible when etched. Common products that implement Damascus steel include knives, guns, and jewelry.

Forge welding is closely related to diffusion welding, where the only real difference between the processes is that plastic deformation is isolated to the joint interface with diffusion welding while plastic deformation is extensive with forge welding. Both processes heavily rely on intimate contact of faying surfaces through plastic deformation, lattice and grain boundary diffusion mechanisms to achieve coalescence.

1.3 Fusion Welding

Modern fusion welding processes can largely be credited to the discovery of electricity in the early 1800's. By the late 1800's the first electric welding process, Carbon Arc Welding, was patented by Nikolay Benardos and Stanislaw Olszewski [8]. The process leveraged electricity to ionize atmosphere creating an arc between the base material and

electrode, causing local melting of the base material. Further development of the idea lead to the modern arc welding processes we know today, which use shielding gas as the medium to be ionize creating the arc for localized melting. Shielding gas or flux are also used to protect the molten weld metal from oxidization.

Welding processes played a key role in the industrial revolution, as welds could often replace rivets which required excess material for overlapping joints and were susceptible to leaking ship hulls. Welded joints allowed airframes to be lighter than bolted or riveted assemblies. Welding also allowed for superior designed parts to hold higher pressures and temperatures, relative to traditional designs, which allowed the jet age to flourish [1,9].

CHAPTER 2

DIFFUSION BONDING THEORY

2.1 Diffusion Welding Fundamentals

The key idea behind diffusion bonding is to achieve coalescence between substrates with a joint interface that is nearly indistinguishable on a microscopic level. This is generally achieved in a furnace with an integrated hot press, intended to apply an axial load to the weldment while simultaneously being subjected to a heat treatment. The heat treatment is intended to induce the diffusion phenomena across the joint interface and allow substrates to share atoms. The integrated hot press is intended to ensure that the faying surfaces of the substrate come into contact with one another. Hot Isostatic Pressure Welding (HIPW) is the same concept except it uses isostatic pressure rather than an integrated ram. Hot isostatic pressure welding requires all exposed surfaces to be sealed to ensure that a pressure difference exists. Theoretically these diffusion welding processes produce a very high-quality joint with uniform mechanical properties.

While elevated temperatures assist diffusion, it also fosters the formation of oxide layers on the substrates surface which hamper diffusion. For this reason, a controlled atmosphere must be maintained to prevent oxides from forming at high temperatures. Hard vacuum is preferred, as some oxides often have a low vapor pressure and will sublime when subjected to high temperatures at high vacuum levels. Interlayer materials, having a low vapor pressure constituents such as silver, will sublime at bonding temperature in high vacuum [5]. This makes bonding in a partial pressure inert atmosphere preferred in these cases to prevent contaminating the vacuum furnace. In these cases,

precautions must be implemented to ensure ultra-high purity of inert gas is used. Moisture content is one consideration that makes bonding in a partial pressure inert atmosphere generally less preferred than vacuum.

Maitland et al. outlined three generic stages of the Diffusion Bonding process to illustrate the overview of the process's metallurgical mechanisms (Shown in Figure 1) [3]. The first stage is characterized by plastic deformation of surface peaks and asperities to form the initial boundary. Second stage diffusion involves grain boundary migration. Third stage diffusion describes volume diffusion which entails interfacial boundary elimination, pore closures within individual grains, and homogenization of the material [3]. Initial interface boundary formation of first stage diffusion often results in high angled grain boundaries which have higher boundary energies, relative to low angled grain boundaries. As a result

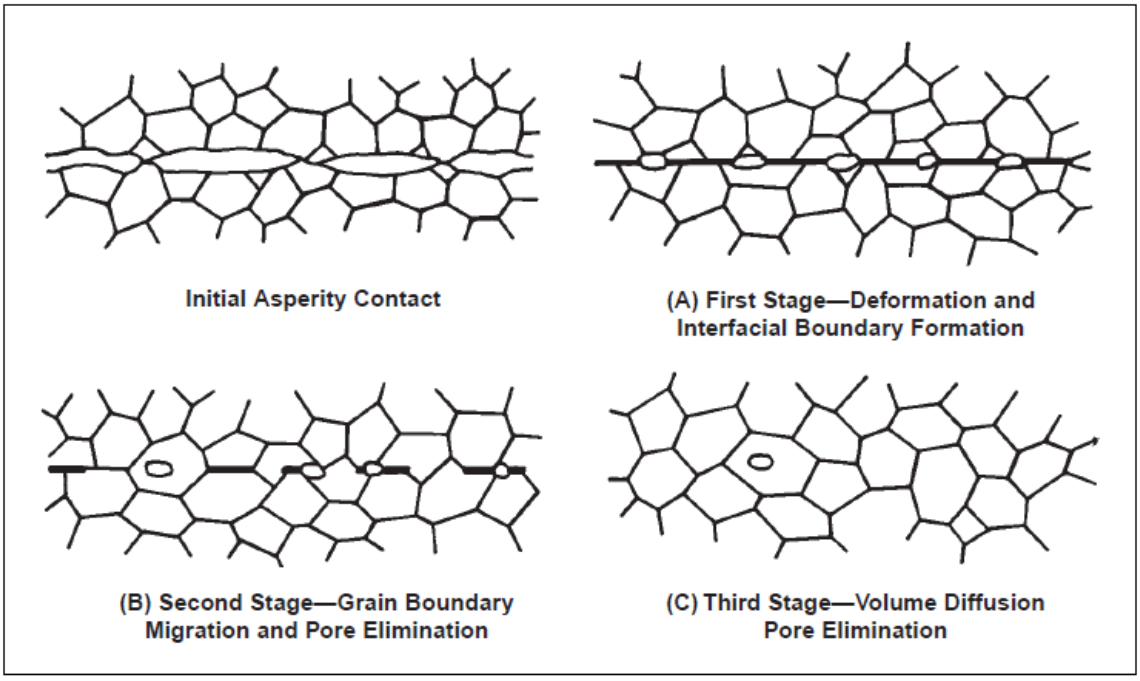

Figure 1: Three Stages of Diffusion Adopted from Maitland et al. [3]

of built-up free energy from plastic deformation and high angled grain boundaries, dynamic recrystallization (DRX) and grain boundary migration can occur at the joint interface [10].

When joining base metals of the same composition, no concentration gradient exists in between the layers. Because of lack of concentration gradients, the bonding process relies on random motion of atoms and random diffusion of atoms via vacancies and other defects. Therefore, random walk theory is an important part of the SSDBW.

2.2 Random Walk Theory

An intuitive example of random movement is Brownian Motion, named after Scottish botanist Robert Brown, which describes the completely random movement of a particles diffusive behavior through a liquid or gas medium. This phenomenon specifically describes movement of particles in liquid or gaseous mediums, which can be impacted by viscosity, density, temperature and molecular mass. It does not apply to crystalline solids and is only mentioned here to give an intuitive visualization of random movement.

(1) $$\Gamma = vzX_v e^{\left(-\frac{\Delta G_m}{k_B T}\right)}$$

$Where$:

$\Gamma = Jump\ Rate$
$\Delta G_m = Activation\ Energy\ for\ Migration$
$T = Absolute\ Temperature$
$K_B = Boltzmanns\ Constant$
$v = Average\ Vibation\ Frequency$
$z = Nearest\ Adjacent\ Site$
$X_v = Probability\ That\ Any\ One\ Adjacent\ Site\ is\ Vacant$ *{applicable only to substitutional diffusing atoms and is omitted for interstitial}*

In crystalline solids, atoms are bound through the crystalline lattice. The crystallographic bonds create a local stress state which is disrupted by the defects in the material. The stress imbalance created by these defects and the random nature of these defects creates a similar random motion which is described by Random Walk Theory (RWT). The random walk theory mathematically describes the jumping motion of atoms based on thermodynamic properties of the material, the vibrational energy needed for an atom to overcome the energy barrier to make a "jump" from one lattice site to another (shown in Figure 2), and the probability that there will be an empty location for that atom to relocate to. The Random Walk Theory is a critical component for describing the element's diffusion coefficient and operates independent of any concentration gradient. Jump rate of substitutional atoms within the crystalline lattice is mathematically modeled with the modified Arrhenius equation (shown in equation (1)) [11,12]. The Arrhenius equation is also where the temperature dependance of diffusion rate is shown. High temperatures increase the mobility of atoms and enhance interdiffusion as described in the activation energy for migration in conjunction with the probability of a neighboring site being vacant. This same equation is used for interstitial diffusing atoms, with the omission of X_v which describes the probability that a neighboring site will be vacant and is based on the mole fraction of vacancies in the metal. Since this study is primarily focused on the movement of substitutional atoms between substrates, the focus of the discussion will be on substitutional diffusing atoms [11].

It is important to elaborate that the activation energy for migration is the minimum change in Gibbs Free Energy required for atoms to overcome the energy barrier required

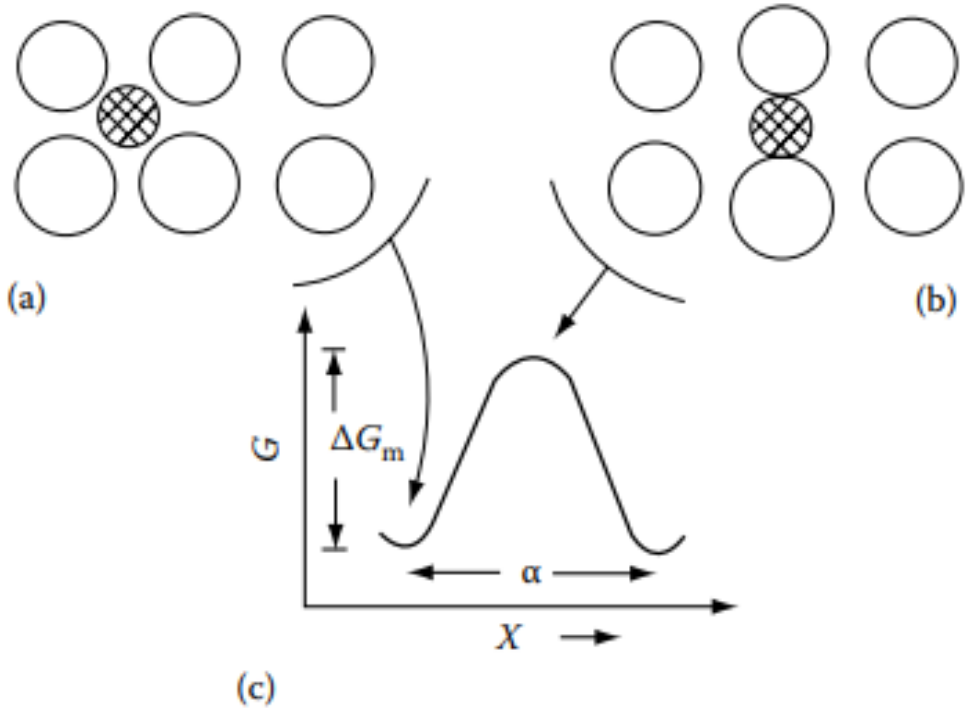

Figure 2: Graphical Illustration of activation energy for migration relative to atom location within the crystalline lattice. (Taken from Porter et. al.)[11]

to make the jump to the neighboring vacant lattice site. Material systems always seek the lowest energy state possible. Temperature is also a key element in the Gibbs free energy equation and is the determining factor in whether the system will favor a higher enthalpy or entropy state. Figure 2, adopted from Porter et.al, generically illustrates the energy change required for interstitial atoms to make the jump between lattice sites [11]. However, this same general relationship also applies to substitutional diffusing atoms with the addition of the term accounting for the probability of the neighboring site being vacant.

Interestingly, the incorporation of Gibbs Free Energy into the random walk theory allows one to draw the conclusion that diffusion rates are sequentially highest at free surfaces,

grain boundaries, and finally within the bulk material. The reason for this conclusion is based on the potential mobility of atoms due to higher levels of entropy at free surfaces and grain boundaries relative to the highly organized bulk. More disordered arrangements of atoms create a lower energy barrier for diffusion to occur. This phenomenon allows grain boundaries to act as highways for atom movement deeper into the substrate relative to the joint interface. This phenomenon termed “grain boundary diffusion” which becomes more critical when interlayer materials are introduced into diffusion bonding process. While grain boundary diffusion happens much faster than bulk diffusion, bulk diffusion still tends to dominate the total volume diffusion. This is largely because grain boundaries will be a much smaller area than bulk grains, relative to the total surface area. Grain boundary diffusion does however coat grains in diffusing atoms which then can

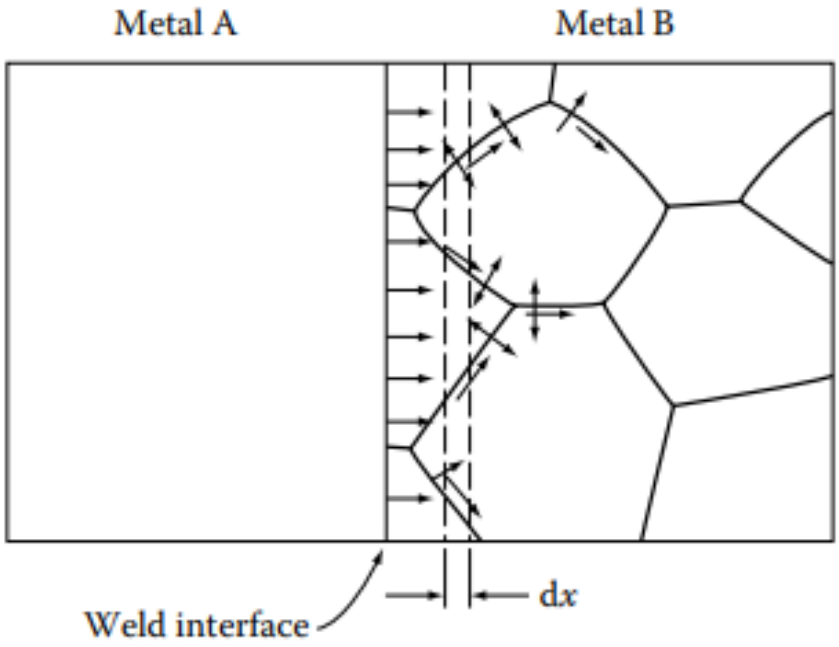

Figure 3: Illustration of grain boundary diffusion. (Taken from Reed-Hill et. al.)

diffuse into the bulk due to more bulk grain surface area being in contact with diffusing atoms as shown in Figure 3 [13].

2.3 Adolf Fick's laws of Diffusion

Fick's first law (shown in equation (2)) outlines steady state diffusion where a flux of "A" atoms passing through a hypothetical datum (represented by J_A) and the intrinsic diffusion coefficient (represented by D_A) both remain constant while the concentration gradient is allowed to change. Fick's first law is not applicable in most practical applications, since the net flux of diffusing atoms will change over time [11]. It is however applicable in applications such as carburizing and hydrogen embrittlement. It could also briefly apply at the beginning of the diffusion bonding process where interlayer materials are used.

$$J_A = -D_A \frac{\partial C_A}{\partial \mathrm{x}} \tag{2}$$

$Where$:

$J_A = \text{Net Flux of atoms Through Hypothetical Plane}$

$D_A = \text{Intrinsic Diffusivity Coefficient of "A" atoms in a "B" atom substrate}$

$$D_A = \frac{1}{6}\alpha^2\Gamma$$

$\frac{\partial C_A}{\partial \mathrm{x}} = \text{Concentration Gradient of "A" Atoms}$

Fick's second law (shown in equation (3)) describes the one-dimensional change in flux of atoms passing through the hypothetical datum as the concentration gradient homogenizes. Fick's second law is more applicable in technical applications, and is very applicable to diffusion welding dissimilar materials or similar materials with the aid of an interlayer material. This interlayer material can be bonded in either the solid state or transient liquid phase (sometimes termed Diffusion Brazing) and is consumed into the

substrate through diffusion [3,14]. The net flux of atoms passing through the hypothetical datum is changing with respect to time as the interlayer is homogenized [11]. A diffusing interlayer material can be plotted as a normal distribution, shown in Figure 4, with the Y axis representing the weight percent interlayer material, with 0 wt% being pure base material and 100 wt% being pure interlayer material, and the X axis represents the positional distance of diffusing atoms into the base material. Homogenizing of the interlayer material into the base material will widen the bell curve, reducing the peak concentration of interlayer material.

$$\frac{\partial C_A}{\partial \mathrm{t}} = D_A \frac{\partial^2 C_A}{\partial \mathrm{x}^2} \tag{3}$$

$Where$:

$\frac{\partial C_A}{\partial \mathrm{t}} =$ Changing Flux of Atoms Through Hypothetical Plane

$D_A =$ Intrinsic Diffusivity Coefficient of "A" Atoms

$D_A = \frac{1}{6}\alpha^2\Gamma$

$\frac{\partial C_A}{\partial \mathrm{x}} =$ Changing Concentration Gradient of "A" Atoms

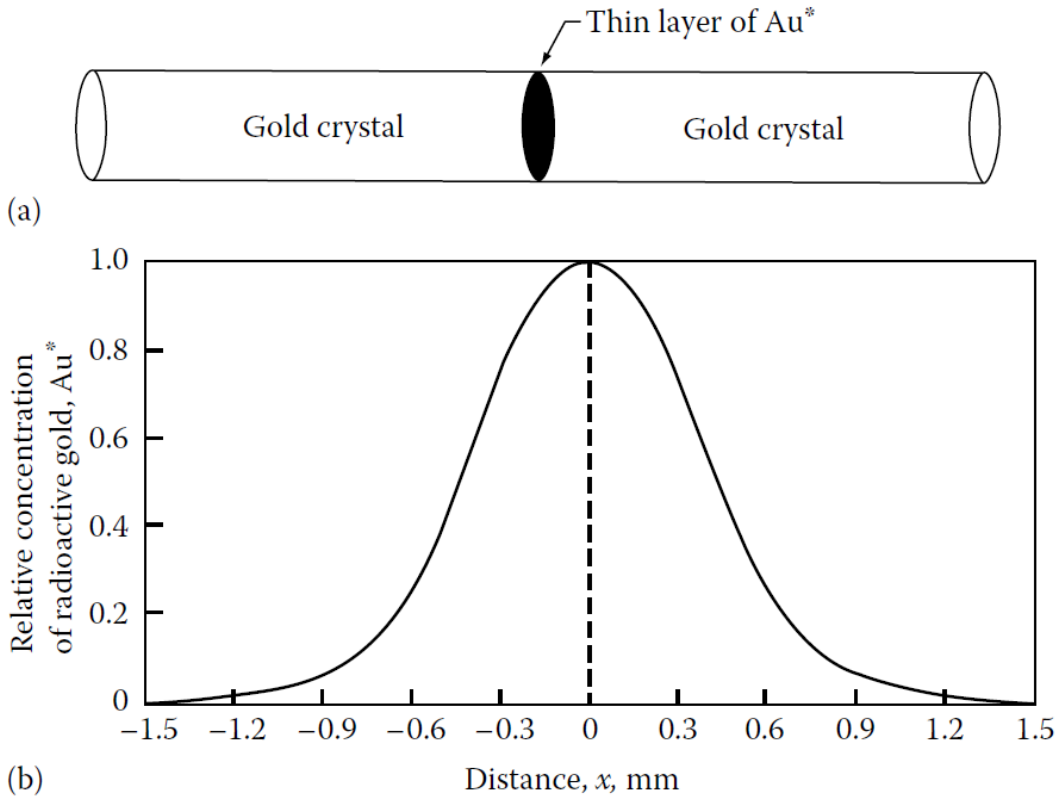

Figure 4: Normal distribution of diffusing interlayer material. (Taken from Porter et al.)[11]

2.4 Surface Finish and Plastic Deformation

If the two substrate surfaces are not touching, there is no opportunity for diffusing atoms to be shared between them. Therefore, consideration of the substrates surface finish must be discussed. Theoretically, two perfectly flat clean surfaces would spontaneously bond without any additional energy applied if brought into contact with one another [2]. This phenomenon is termed Cold Welding and is problematic in designs intended for space applications [6]. In terrestrial reality this is unachievable, on large scales, due to surface imperfections, such as oxides, and microscopic peaks and valleys present on even the best surface polishes. Macroscopic surface parallelism is also another factor to be

considered which can affect surfaces from coming in contact with one another. Oxides and contaminates inhibit diffusion between substrates by creating a barrier with a low intrinsic diffusivity coefficient relative to the base material. Extreme measures must be taken to minimize these imperfections.

Preparing samples for joining can typically take the form of surface grinding, lapping, polishing, and chemical etching substrates prior to welding. It can also be advantageous to cold work the surface of samples [4]. This theoretically deforms surfaces which forces the microstructure into a higher free energy state, relative to the undeformed bulk. One issue with this theoretical method is maintaining an acceptable microscopic surface finish, as post cold work polishing would remove the deformed material making this practice moot. Macroscopic surface parallelism and microscopic surface finish should be monitored prior to bonding with a maximum allowed surface parallelism established.

Some of the surface imperfections are remedied by using high temperature and pressure during the diffusion bonding process. A best practice for diffusion welding is to select temperatures and pressures, ideally within the materials Nabarrow-Herring Creep range and slightly below the materials yield point, which theoretically isolates plastic deformation to the joint interface. This is because as point loaded surface asperities are crushed against one another the area in contact is increased, effectively reducing the stress at a fixed loading condition. This phenomena continues until the prescribed pressure is asymptotically approached. Hill et al. described this as stage 0 of the diffusion bonding process [15]. A simple scenario of this theory is modeled in Figure 5. By assuming

linear surface scratches, from substrate preparation, having a defined surface roughness (RA) equal to the radius of the polishing media used. It was also assumed that the surface asperities were in perfect parallel alignment, which is known to be highly unlikely. By using the modified the equation of a circle (solving for x), shown in equation (4), the origin of the circle, (h,k) is systematically changed by allowing k to increase to k=r while h is held constant. This model assumes that plastic deformation will cause the surface pores to deform at contacting surfaces and reduce the volume of each pore. This close contact provides an opportunity for atoms to cross the interface. It should be noted that this model approximates void closures observed and omits diffusion and creep mechanisms from consideration. This model is only shown to stress the point that constraining plastic deformation to the joint interface is critical for diffusion welding.

(4) $$A = 2 * \left(\sqrt{r^2 + \left(\frac{dk}{dt}\right)^2} + x_0 \right) * L$$

$Where$:

$A =$ Contacting surface area

$r =$ average surface rougness (assumed to be the radius of polishing media)

$\frac{\mathrm{dk}}{\mathrm{dt}} =$ y component of the surface imperfection with respect to time

$x_0 =$ origninal contacting surface length

$L = Length\ of\ the\ coupon$

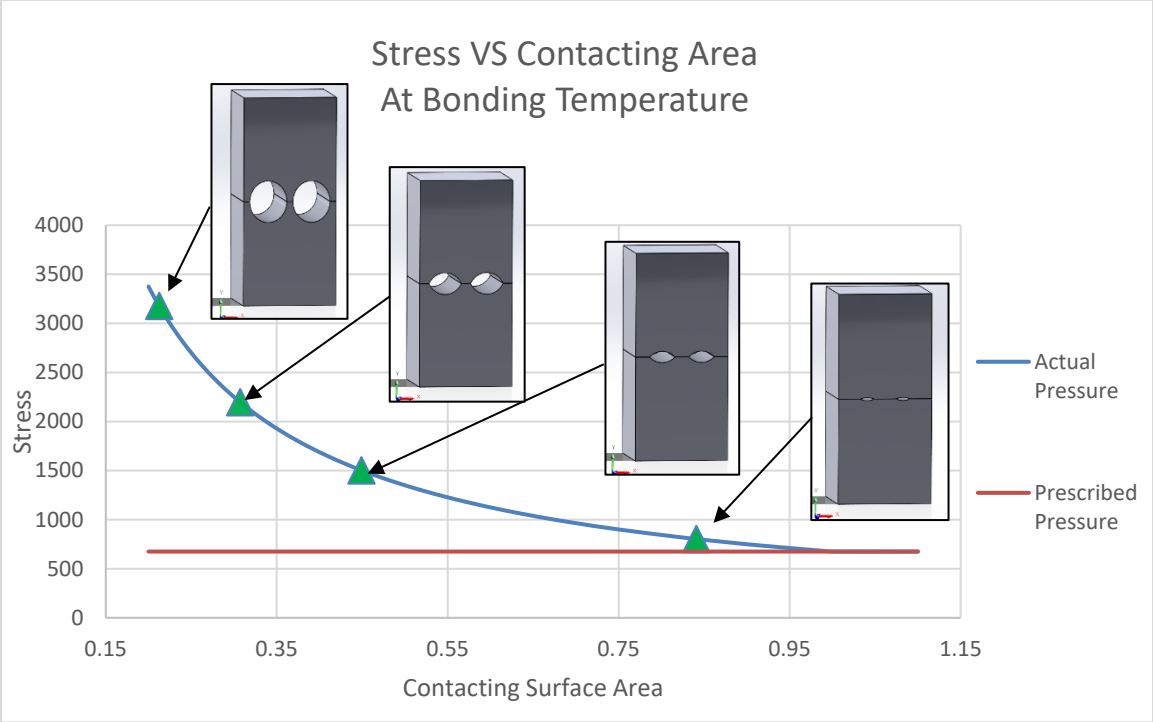

Figure 5: Change in Stress as a Function of Pore Closure

Derby et al. proposed a more rigorous model, based on similar studies completed for sintering applications, where the three general stages of diffusion were modeled individually. Interestingly, the scratch geometry that was used was a triangular in shape. Variables such as diffusion coefficients and bonding temperature were used to establish the rate of change of volume with respect to time [16]. Later, Hill et. al further built on this model, by further breaking down the diffusion bonding process into six generic sub categories and by using eliptical voids, rather than triangular. This study adds a stage 0 into the process that acknowledges plastic deformation, occuring at the joint interface due to a localized yielding stress applied, will cease once the contacting areas are sufficiently large to support the applied load. Strage 1, 2, 3 describes surface diffusion, volume diffusion and mass transfer by evaporation, respectivly, from the contacting surfaces as

asparities are necked. Stages 4 and 5 describe grain boundary and bulk diffusion respectively. Stage 6 describes power law mico creep, which is undesirable due to the deformation of the sample [15].

CHAPTER 3

NICKEL-BASED ALLOYS

3.1 Background of Nickel-Based alloys

Nickel-based alloys are known for their excellent corrosion resistance and mechanical properties at elevated temperatures. The alloys are extensively used in aerospace, naval, chemical processing, and oil and gas applications for their ability to resist harsh environments and aggressive chemicals needed for refining chemical products. They are also extensively used in turbine and rocket aerospace engines for their excellent performance at temperatures well above 60% of their melting temperatures. The jet age and modern commercial and military air travel would not be possible without nickel-based superalloys. Lippold et al. broadly categorized nickel-based alloys into four groups as follows [1].

- Commercially Pure: Commercially pure alloys that have limited use due to their relatively low strength and are mostly limited to applications in electrical, magnetostrictive, and corrosion applications.
- Solid Solution Strengthened: These alloys are generally the most widely used in industry for their good strength and corrosion resistance. Monels and Cupronickels are an example of solid solution strengthened alloys. These alloys primarily use copper as an alloying element, since copper is very thermodynamically compatible with nickel. These alloys are extremely capable of resisting sea water corrosion and are extensively used in offshore oil rigs and naval applications. Other solid solution alloys with primary alloying elements of

Chromium, Iron and Cobalt are used where precipitation hardening characteristics are less desirable or not needed.

- Precipitation strengthened: The alloys in this category leverage highly reactive elements such as Aluminum, Titanium, and Niobium for alloying the bulk that can form strengthening precipitates. These alloys are particularly effective in fatigue and creep critical applications such as turbine and rocket engines. Precipitation strengthening is often credited with doubling some materials yield strength. Generally, there is a notable sacrifice in ductility for the gain in extra strength.
- Other Specialty Alloys: Some of these specialty alloys are specially designed for creep and fatigue applications and generally leverage precipitation strengthening as well as dispersion hardening characteristics.

3.2 Inconel Alloy 718

The focus of this research is on Inconel 718, which is a polycrystalline solid solution strengthened FCC alloy with additional precipitation strengthening from the intermetallic phases of γ" (Body-Centered Tetragonal Ni_3Nb) and trace amounts of γ' (Face-Centered Cubic $Ni_3(AL, Ti)$) [17]. γ" precipitate typically take a disk-shaped geometry while γ' are cubic in shape. Other less desirable precipitation mechanisms exist in the alloy such as the existence of Laves and δ phase (Orthorhombic Ni_3Nb) which have both been shown to be detrimental to mechanical properties. δ phase can however be leveraged for some advantageous applications such as controlling grain growth and improving the alloys

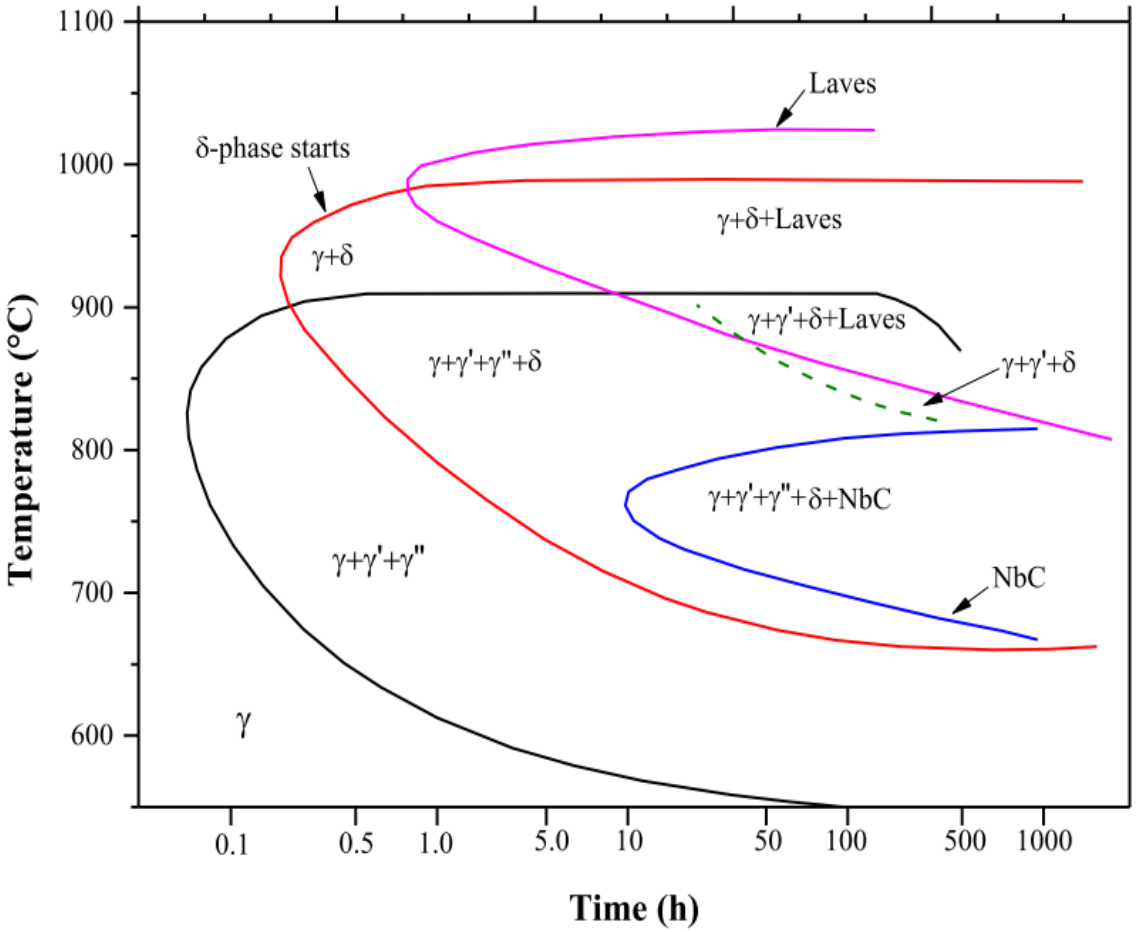

Figure 6: Time-temperature-transformation (TTT) diagram of Inconel 718 (Adopted from Thompson et al.)

fatigue life by pinning grain boundaries ultimately restricting mobility of grains under load [18]. This improvement in fatigue life comes at the expense of some ductility and a marginal decrease in yield strength. The decrease in yield strength is theoretically attributed to delta phase requiring some percentage of Niobium, tying up precipitation forming elements. The NbC and TiN precipitates also can visually be seen through the material and generally exist from the mill. Figure 6 shows the time temperature transformation diagram (TTT) for alloy 718's precipitation phases and their corresponding formation temperature range, adopted from Thompson et al [19]. The alloy

obtains its solid solution strengthening from the addition of Chromium, Iron, and trace amounts of Molybdenum and Cobalt as shown in the alloys composition in Table 1, taken from AMS5662 [20]. The alloy has limited use in the solution heat treated condition, however, can still be used in the solution heat treated condition when the application allows the reduction in yield strength. US patent No. 3,046,108 was granted in 1963 for the invention of Inconel Alloy 718, by H. L. Eiselstein of the International Nickel Company (where the alloys, and similar alloys, get their nickname Inconel) [21]. The alloy has been extensively used in the aerospace industry due to the materials-excellent mechanical properties at elevated operating temperatures. Alloy 718 combines the desired ductility properties of solid solution alloys with the addition of precipitation strengthening elements.

Element	**Minimum Composition**	**Maximum Composition**
Chromium	17.00	21.00
Nickel	50.00	55.00
Iron	Ballance	
Molybdenum	2.80	3.30
Columbium (Niobium)	4.75	5.50
Titanium	.65	1.15
Aluminum	.20	.80
Cobalt	-	1.00
Other trace elements may exist but are limited to maximum quantities.		

Table 1: Inconel 718 Chemical Composition (Taken from AMS5662)

The alloy is known to be relatively processable with good weldability relative to other precipitation hardenable alloys. The sluggish precipitation of γ" aids the alloy in resisting the strain age cracking phenomenon that makes other precipitation hardenable alloys (such as Rene 41, Inconel 939, and Rene 80) considered unweldable [1]. Casting and LPBF additive manufacturing also benefit from this same phenomenon. Inconel is also known to be machinable with relative ease. It is preferred to machine in the solution heat treated condition, but it can also be done in the aged condition.

Alloy 718 is known to be a very versatile material and can exhibit a variety of mechanical properties depending on the type of heat treatment applied. The alloy, in the wrought form, boasts a 70 ksi yield in the solution heat treated condition and has extensive strain hardening capabilities in this condition. This yield strength easily increases to 160 ksi when subjecting the material to an AMS2774 condition S1950DP heat treatment while still achieving a minimum elongation of 12%. The AMS2774 condition S1750DP heat treatment leverages the precipitation of some δ phase at grain boundaries, effectively pinning grain boundaries, which locks the microstructure in place improving fatigue properties. Increasing the fatigue properties comes at the price of reducing the yield strength to 150 ksi due to δ phase consuming some precipitation forming elements [20].

This polycrystalline alloy has also been shown, by Ruan et al., that grain size has a crucial role in Inconel 718's yield strength as outline by Hall-Petch [17,22]. Some studies have shown that δ phase precipitated at grain boundaries can aid in controlling grain

growth below super solvus temperature. This could theoretically be leveraged to control grain growth of the material during diffusion bonding [18]. Guoge et al. conducted experiments diffusion bonding Inconel 718 in the precipitation hardened condition. They completed the diffusion bonding in a vacuum hot press and utilized high loading conditions relative to this study. The temperatures they used ranged from just below and just above super solvus solution heat treatment temperature ranges but were all above the solvus temperature for γ" and γ'. There is no indication in the report that any post-weld heat treatment was implemented on the substrates. Metallographic results of their study showed incomplete recrystallization of the joint interface. Tensile results reported were shown to increase logarithmically with increased temperature. The author did not specify if yield or ultimate tensile strength was reported, so it is assumed that ultimate tensile strength results are reported which do not exceeded the expected properties of Inconel 718 in the solution heat treated condition [23,24].

CHAPTER 4

SOLID STATE DIFFUSION BONDING EXPERIMENT

4.1 Experimental Testing Methods

Inconel 718 bar, compliant to AMS5662, was sectioned into 1.25 inch (31.75 mm) long sections with a section saw. After sectioning, samples bond surfaces were polished via general metallographic polishing equipment to 1200 Grit paper. A vibratory polisher was then used to achieve the final surface finish which was iteratively varied. Since surface finish is an essential variable to the process, a Veeco WYKO NT1100 interferometer was used to measure the microscopic surface finish. Individual readings were documented and can be found in table 1. Samples were cleaned in an Acetone bath with ultrasonic agitation for a duration of 15 minutes. In an attempt to minimize oxide formation, samples were placed into vacuum furnaces within 60 minutes of final polishing.

Welding took place in a Centorr Vacuum Furnace with an integrated hot press that complied to the requirements of AMS 2750 [25]. The integrated hot press was designed to maintain a constant loading by varying ram displacement. The furnace was equipped with data acquisition technology with thermocouples and sensors integrated to record essential bonding parameters at a sampling rate of two readings/minute for the duration of the bonding cycle. Values recorded include actual temperature, applied load, vacuum level, power usage, and ram displacement and can be seen in appendix A. High vacuum levels of 10^{-4} Torr were used until a temperature level of 500°C (932°F) was reached then ultra-high purity argon backfilled the chamber. An argon backfill was also used as means of quenching the samples at the end of the bonding cycle. The furnace operator mistakenly

selected the wrong program on SN 5 and completed bonding of this sample under high vacuum. As a result of the incorrect program being selected, the argon backfill was not used for quenching sample 5. Tungsten tooling blocks were used to minimize tooling distortion and wear. A ceramic spacer was used so that the tooling would not bond to the sample.

Sample ID	Surface Finish RA µm (µin)		Diffusion Bonding Parameters					
	A	B	Temperature °C (°F)	Soak Time (hours)	Pressure Mpa (psi)	Atmosphere	ASTM Grain Size Number	Yield Strength Mpa (KSI)
Control	N/A	N/A	N/A	N/A	N/A	N/A	3.77	(148.5)
SN0	N/R	N/R	1175 (2147)	4	4.653 (675)	99.9997% Ar	1.64	-
SN1	7.74 (304.7)	6.04 (237.8)	1175 (2147)	8	4.653 (675)	99.9997% Ar	.799	-
SN2	4.23 (169.3)	4.64 (182.7)	1175 (2147)	8	11.032 (1600)	99.9997% Ar	.43	-
SN3	1.76 (69.3)	1.08 (42.5)	1175 (2147)	8	6.895 (1000)	99.9997% Ar	-.58	-
SN4	0.1 (3.39)	0.09 (3.54)	1225 (2237)	8	5.861 (850)	99.9997% Ar	-1.705	(111.03)
SN5	0.14 (5.51)	0.14 (5.51)	1225 (2237)	5	5.861 (850)	High Vacuum	.082	(143.09)
SN6	0.09 (3.54)	0.12 (4.72)	1225 (2237)	4	5.861 (850)	99.9997% Ar	-2.49	(110.68)
SN7	0.11 (4.33)	0.11 (4.33)	1130 (2066)	4	11.032 (1600)	99.9997% Ar	2.119	(114.54)
SN8	.097 (3.82)	.067 (2.637)	1175 (2147)	4	11.032 (1600)	99.9997% Ar	-1.26	(124.478)

- indicates the test was not performed.
*N/A indicates not applicable.
**N/R indicates data was not recorded.

Table 2: Bonding Parameters and Testing Results

Several combinations of bonding parameters were tested and are outlined in Table 1. Since the goal of these experiments was to establish solid state bonding parameters that achieved complete grain coalescence without the aid of an interlayer materials, parameters were not varied systematically. Rather they were iteratively varied to establish an acceptable solid state diffusion bond. Since one of the key research goals was to have

as little distortion as possible, relatively low loading was implemented ranging from 4.65 mpa (675 psi) – 11.03 mpa (1600 psi). Per previous research, bonding temperatures were kept above solution temperature to avoid the precipitation of δ phase [23,26]. Soak times were based on previous experience and literature review.

After bonding, one transverse test specimen was removed from the sample for metallographic evaluation in the as-welded condition. A second metallographic sample was taken after precipitation heat treatment for comparison and taking micro hardness measurements. Metallographic samples were prepared by sectioning bonded samples and mounting them in epoxy resin then grinding, polishing to .05µm RA, and etching with 10% oxalic acid aided by 5-volt electrolytic anode/cathode. A Keyence VHX-X1 digital microscope was used for metallographic analysis with magnifications ranging from 20X to 1200X. The samples were evaluated to ensure that proper coalescence between the two substrates was achieved with adequate grain crossing and pore closures. Definition of acceptable grain crossing and pore closure was left relatively ambiguous to understand what is possible, however the goal was for the resultant joint interface to essentially be unseen. Grain size measurements were taken using the Lineal Heyn Intercept Technique and converted to ASTM grain size number. The resultant grain size measurements were compared to the base material in the precipitation hardened condition. Individual NbC and TiN precipitates were randomly measured, using a Keyence VHX-X1 digital microscope, to establish and average precipitate size.

When an acceptable bond was characterized in metallography, the sample was subjected to a two-step precipitation heat treatment in accordance with AMS2774 condition S1750DP in a vacuum furnace [27]. A data acquisition system was used to monitor the heat treatment cycle and can be found in appendix A. The data acquisition system had an error on Sn8 and as a result did not start collecting data until about halfway through the cycle. Since bonding temperatures exceeded the solution heat treat condition, another solution heat treatment was omitted from the process. Even though the temperature ranges were well below the δ phase precipitation curve, shown in Figure 6 argon gas quenching was used to control cooling rates.

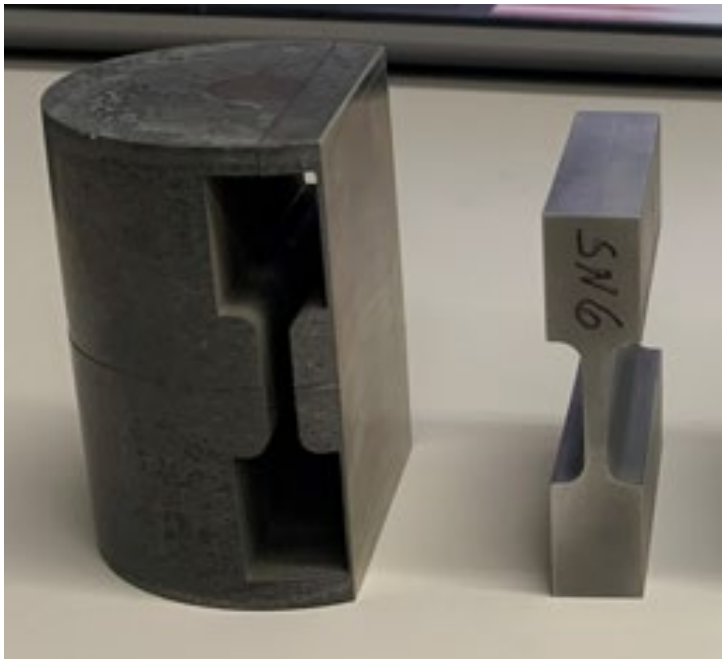

Figure 7: Location of Tensile Samples Relative to Weldment

A Tescan Vega scanning electron microscope was used to analyze metallographic samples to identify precipitates and look for relevant indications that can be difficult to

see with optical metallography. Scanning electron microscopy energy dispersive x-ray spectrometry (SEM-EDX) was used to characterize the chemical composition of secondary phases. In order to ensure the samples surface was adequately conductive, mounted samples were gold plated using the sputter vapor deposition technique. Copper tape was also applied to a corner of the sample's surface and then connected to the fixturing to ensure conductivity. Samples were observed using both backscatter and secondary emission technique. EDX analysis of precipitates was implemented to characterize the locations of interest and surrounding areas.

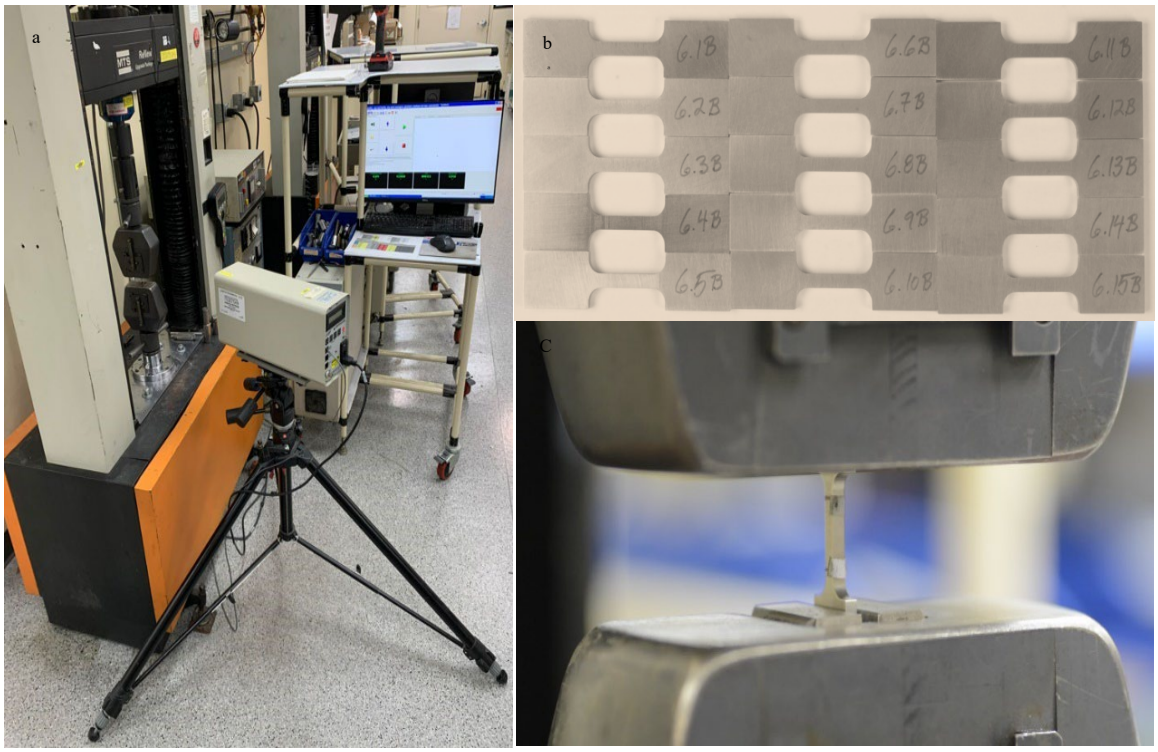

Figure 8: Tensile Testing Configuration

a. Instron Tensile Tester with Epsilon Laser Extensometer
b. Miniature Flat Tensile Sample Profile View (8X Magnification)
c. Miniature Flat Tensile Sample in Testing Jaws (5X magnification)

The wire EDM process was used to remove miniature flat tensile samples, compliant to ASTM E8, from the weldment with the joint interface located in the approximate center of the gauge (see Figure 8 for reference). The gauge of the single blanked samples was carefully polished by hand with 600 grit sandpaper to remove any recast layer from the wire EDM process with micro scratches going in the direction of loading. Once recast was removed, the sample was taken back to the wire EDM machine to remove a minimum quantity of 10 samples, 2.616 mm (.103 in) thick, from the blanked sample. Recast was again carefully removed from the sample by hand polishing with 600 grit sandpaper with micro scratches going in the direction of loading.

Tensile testing was conducted using an Instron load cell in conformance to ASTM E8 at room temperature (see Figure 7 for setup configuration). It was determined that the load cell and tensile samples worked best utilizing crosshead speed controls (ASTM E8 Control Method C) with a strain rate of .05 in/in/min which was implemented on all samples tested [28]. A laser extensometer, in conjunction with reflective tape, was used to collect strain data. Ten samples were tested for each experiment a summary of the results are shown on one curve fit that captured average modulus of elasticity, yield strength, ultimate tensile strength, strain at fracture, as shown in Figure 11.

After metallography data was collected, metallographic samples, in the polished and etched condition, were subjected to a micro hardness survey. A Struers Duramin-40 AC1

was used to collect Vickers .05 kg (HV.05) microhardness data. The automated machine collected data in four traverses, across the joint interface, per sample taken perpendicular to the joint interface. Each traverse contained five indentions for a total of twenty microhardness readings per weldment. Each indentation was manually checked to verify proper measurements of the indentation. The values were averaged to obtain the weldments microhardness.

To have a control material for comparison, one unbonded base material substrate was subject to a super solvus solution heat treatment and precipitation heat treated in accordance with AMS2774 condition S1750DP and subjected to metallography, hardness, and tensile testing (ten samples). The same sample preparation procedures and sample sizes described above for metallography, microhardness and tensile samples was used on this control sample as were used on the bonded samples.

4.2 **Results and Discussion**

First stage mechanism suggests that free surfaces quickly begin sharing atoms where contact is made and become more restricted to atom movement, similar to diffusion within the bulk, as bonds are formed. Grain boundary diffusion rates dominate at lower temperatures due to highly disordered packing resulting in lower activation energy [4]. Grain boundary migration, driven by the minimization of boundary energy, tends to align and result in elimination of the joint interface. This alignment of grain boundaries is described as second stage diffusion shown in Figure 1. Third generic diffusion bonding process stage involves plastic deformation allowing intimate contact between surfaces and forces unbonded surfaces and micro pores to be eliminated. Complete coalescence consists of two materials that are nearly indistinguishable from one another where the joint interface cannot easily be seen.

Looking at the metallographic images of the bonds and relating to the parameters that were used for each test, it appears that surface roughness plays a very critical role to the extent that it overshadows other parameters such as temperature and pressure. This is further compounded since relatively low loading is required to isolate plastic deformation to the joint interface. Plastic deformation can damage intricately cut sheet components that when stacked together can affect the design intent of the sheet laminate additive manufacturing process. Figure 8 shows that the joint interface only starts to disappear when the surface roughness is reduced to 0.2 micrometers. Metallographic inspection revealed that varying stages of diffusion had taken place as outlined in Figure 8. Sn0

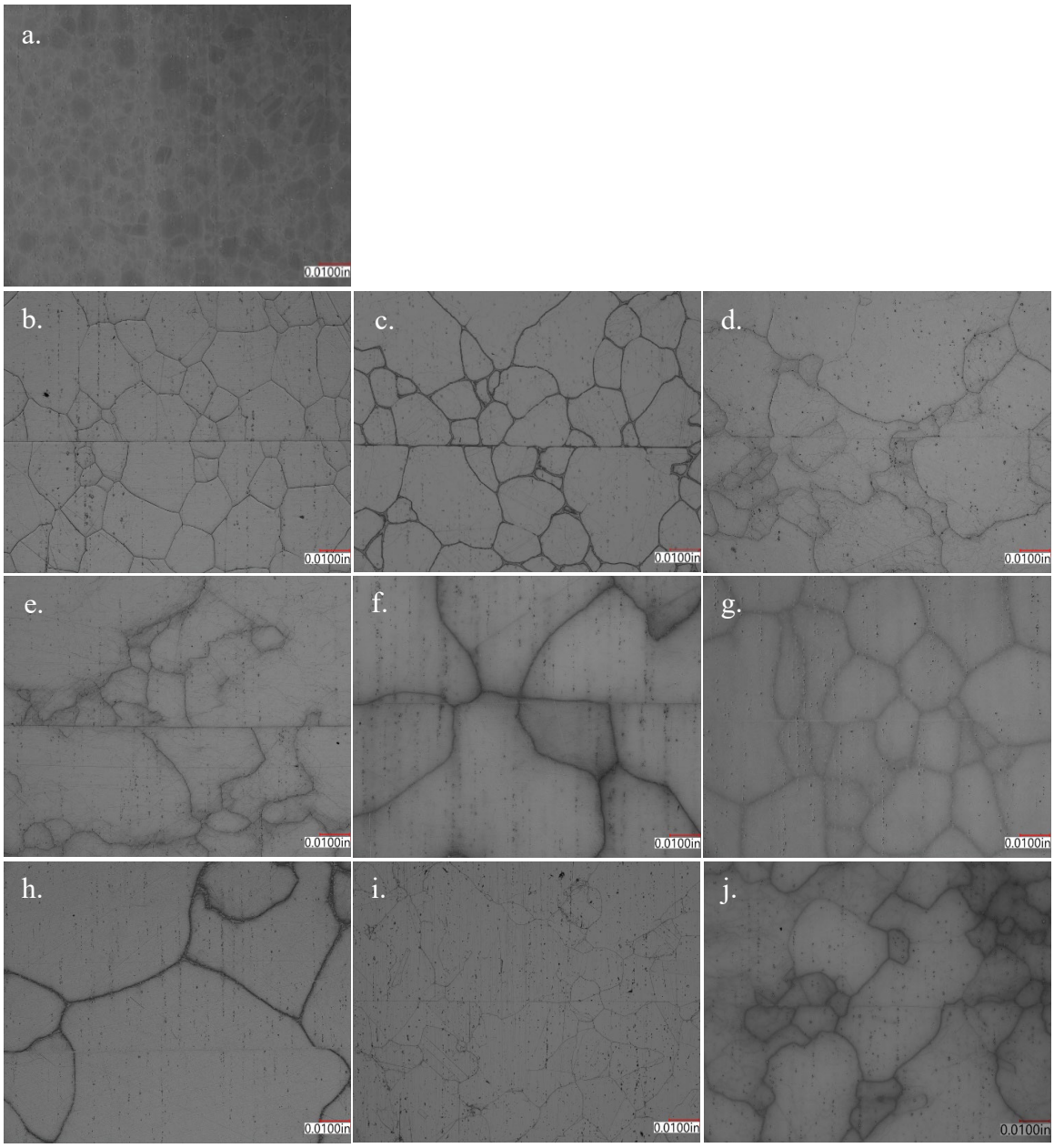

Figure 9: Metallographic Evaluation of Bonded Joints at 100X Magnification

Control sample

SN0 (Bonded at 1175°C for 4 hours, RA was not recorded).

SN1 (Bonded at 1175°C for 8 hours, RA was<7.74µm).

SN2 (Bonded at 1175°C for 8 hours, RA was<4.64µm).

SN3 (Bonded at 1175°C for 8 hours, RA was<1.76µm).

SN4 (Bonded at 1225°C for 8 hours, RA was<.1µm).

SN5 (Bonded at 1225°C for 5 hours, RA was<.14µm).

SN6 (Bonded at 1225°C for 4 hours, RA was<.12µm).

SN7 (Bonded at 1175°C for 4 hours, RA was<.11µm).

SN8 (Bonded at 1130°C for 4 hours, RA was<.11µm).

achieved stage 1 diffusion, since initial contact was made but grain boundaries were not aligned. Sn1, 3 had some grain crossing which by definition achieves stage 2 diffusion. SN 2 had good grain crossing and pore closure, however the sample had excessive distortion. It was not until the average surface roughness (RAμm) was decreased to under .2μm (7.874 μin) that acceptable stage 3 diffusion was achieved on samples 4, 5, 6, 7, and 8.

As temperature increases, mobility of the atoms increases resulting in higher diffusion rates as dictated by Ficks Laws [11,12]. However, increasing temperature can also result in recrystallization and grain coarsening at temperatures above recrystallization temperature for Inconel 718. Recrystallization temperature for Inconel 718 varies and it could be as low as 1150°C. Samples bonded at 1225°C (2237°F) were consistent with this and had excellent diffusion and pore closure. However, as expected grain recrystallization and coarsening also occurred as these samples had a negative ASTM grain size number which indicates very large grains. Experiments (SN7 and SN9) were conducted at lower temperatures, 1130°C (2066°F) and 1175°C (2147°F) respectively, with higher loading intended to achieve intimate contact between substrates faster. These tests resulted in a positive ASTM grain size number while still achieving adequate coalescence and marginal micro pore closure. As previously stated, some studies have shown that δ phase can be leveraged to control grain growth [18]. While this could theoretically be leveraged to control the grain growth, other considerations such as recrystallization would suffer as a result of bonding at temperatures where δ phase is stable. This theory could potentially

use both these phenomena separately with a more complex bond cycle, which was outside the scope of this research.

While every effort to ensure substrates had a clean, oxide free surface, some samples has visual evidence of a thin oxide layer was observed in metallography. The AWS brazing handbook recommends nickel plating material containing notable amounts of highly reactive elements, such as titanium, aluminum and magnesium, prior to brazing in an effort to prevent oxide formation which inhibit diffusion of braze filler material melting point depressants.[2] While this practice was outside the scope of the experiment, an interlayer material would likely aid the bonding process by removing the oxide layer challenge associated with achieving diffusion between substrates.

A closer look at the microstructure through SEM EDX and EBSD analysis revealed existence of large Niobium rich carbide and Titanium rich nitride precipitates, throughout all the samples including the base material as well as bonded samples. It was observed that in some instances, these carbides were linearly aligned with the roll direction, as shown in Figure 9 and Figure 10. Ostwald Ripening, of Niobium rich carbide and Titanium rich nitride precipitates was observed in all processed samples, including the unbonded base material in the precipitation heat treated condition, to varying degrees [17]. Precipitates displayed elevated levels of Nb and C in the form of white particles in the matrix while black precipitates contained Ti and N as shown in Figure 10. Ostwald Ripening is a thermodynamically driven diffusion-controlled precipitation growth mechanism where large precipitates grow larger at the expense of smaller precipitates,

driven by the higher interfacial energies associated with smaller precipitates. It is shown that elevated temperatures are required to achieve volume diffusion also expedites diffusion required to cause undesired precipitation growth. This effect can theoretically deplete the crystalline lattice of valuable elements required to form γ" and γ'. This is further complicated since Niobium and Titanium are extremely reactive elements and are incredibly stable in NbC and TiN form, making dissolving these precipitates nearly impossible. Ruan et al showed that dissolving NbC precipitates required temperatures near Inconel 718's melting temperature, 1280°C (2340°F). The study showed that TiN would still exist at liquid temperatures and would gradually be dissolved by liquidus phases [17].

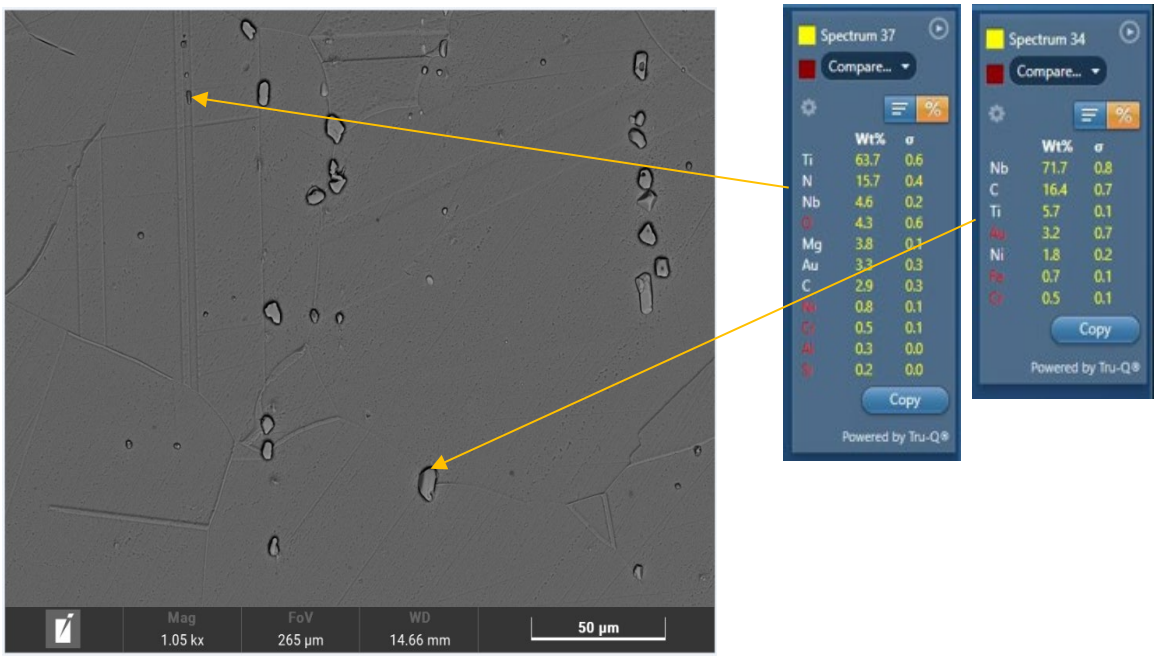

Figure 10: SEM Analysis of Precipitates in Unbonded Base Material

A proper balance between achieving coalescence at the joint interface and maintaining a fine grain size in the substrate as well as avoiding Ostwald Ripening is a challenge as

diffusion, which is a temperature driven mechanism, is the cause for all these phenomena. It can be concluded that some amount of grain growth would be required to achieve volume diffusion and grain migration across the joint interface, since it is only possible to refine grain size on nickel-based alloys through cold working. This effect can be accounted for in the design's calculations.

As a result, a reduction in mechanical properties must be considered due to grain growth per the Hall-Petch theory (shown in equation(5)) and diffusion-controlled Ostwald Ripening [22]. This point is further complicated in Inconel 718 since the detrimental δ phase has been shown to precipitate between 700°C (1292°F) – 1000°C (1832°F), which bounds the lower temperature at which diffusion bonding would be practical without complex bonding cycles.

(5) $$\sigma_y = \sigma_0 + \frac{k_y}{\sqrt{d}}$$

$Where$:

$\sigma_0 = material\ constant\ \{resistance\ of\ dislocation\ movement\}$

$k_y = material\ strengthening\ coefficient$

$d = average\ grain\ diameter$

Mechanical tests were conducted at room temperature to the point of failure to evaluate the elastic and plastic mechanical behavior. The base material displayed an average Youngs Modulus of 23 Mksi, yield strength of 1013.94 Mpa (148.57 ksi) at 2% offset, ultimate tensile strength of 1243.12 Mpa (181.4 ksi), and 31.84% elongation which closely align

with the published data of AMS5662 [20]. The base material's tensile properties were very consistent showing a yield strength standard deviation of 1.57.

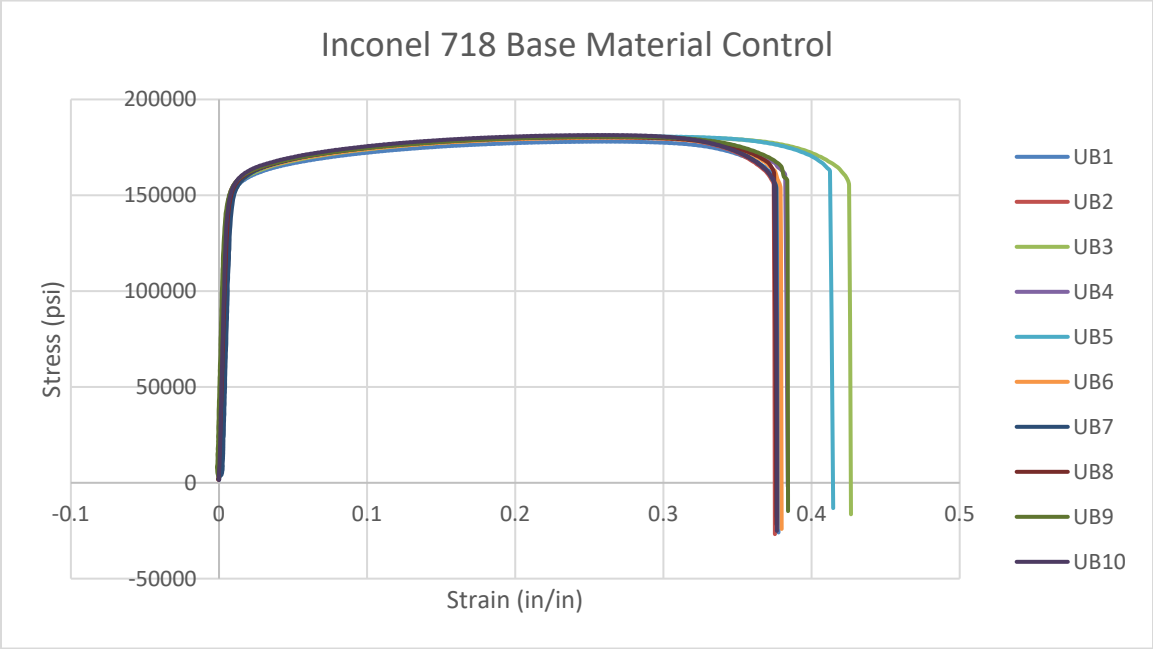

Figure 11:Inconel 718 Base Material Control Sample Tensile Test Stress Strain Curves (in the AMS2774 1750 heat treat condition)

Diffusion bonding parameters had a drastic impact on the weldment's mechanical properties indicating that rigorous development and qualification of parameter must considered in the development process. All samples bonded in argon atmosphere displayed reduced yield, UTS and elongation while samples bonded in hard vacuum (where the argon atmosphere was not turned on by mistake) (SN5) displayed yield strengths similar to the base material. In most samples brittle fracture occurred in the joint interface exhibiting a lower ductility. Figure 12 displays representative average stress strain curves for each weldment. This representative average is based on the average of all ten tensile samples

tested from each sample. Each of the samples actual stress strain curves can be found in appendix B. All samples displayed strain hardening to varying extents. The reduced strength can be theoretically related to the Hall-Petch effect due to grain coarsening that occurs during bonding. Metallography of the control sample displayed significantly smaller grain sizes than any of the samples bonded.

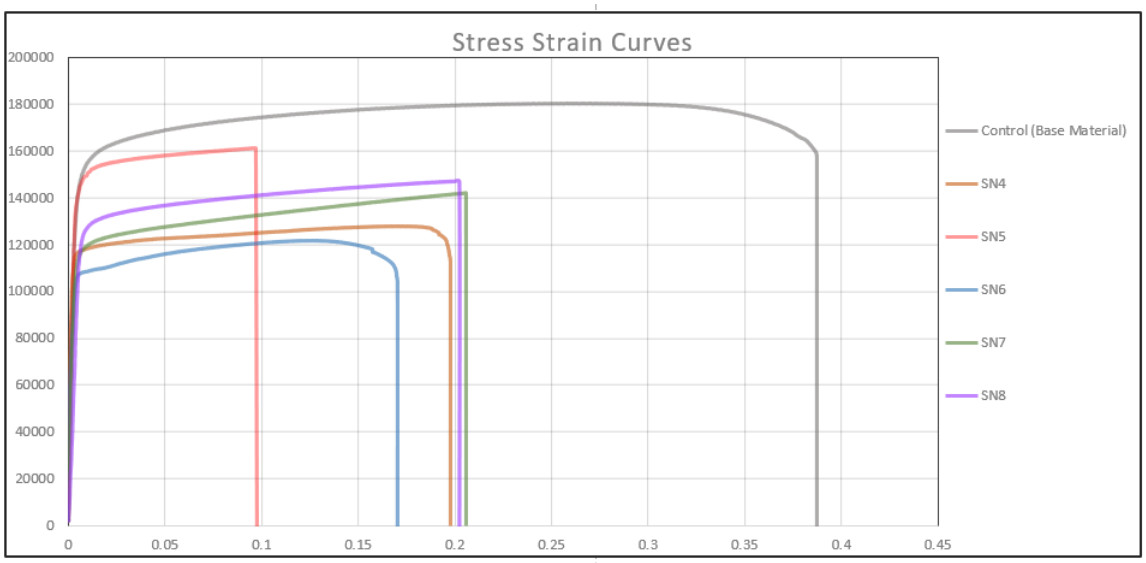

Figure 12: Representative Average Stress Strain Curves of Weldment Population {X axis: Strain (in/in), Y axis: Stress (psi)}

Optical microscopic analysis of tensile samples metallography, shown in Figure 13, indicated that plastic deformation of all samples appears to be uniform through the tensile samples gauge. This is consistent with the theoretical advantage of diffusion welding having uniform mechanical properties, similar to the base material. Samples that displayed brittle fracture had significantly less plastic deformation due to the premature failure in the joint interface. Premature fracture could theoretically reduce ultimate tensile strength values due to the test being interrupted before samples become fully strain hardened. When

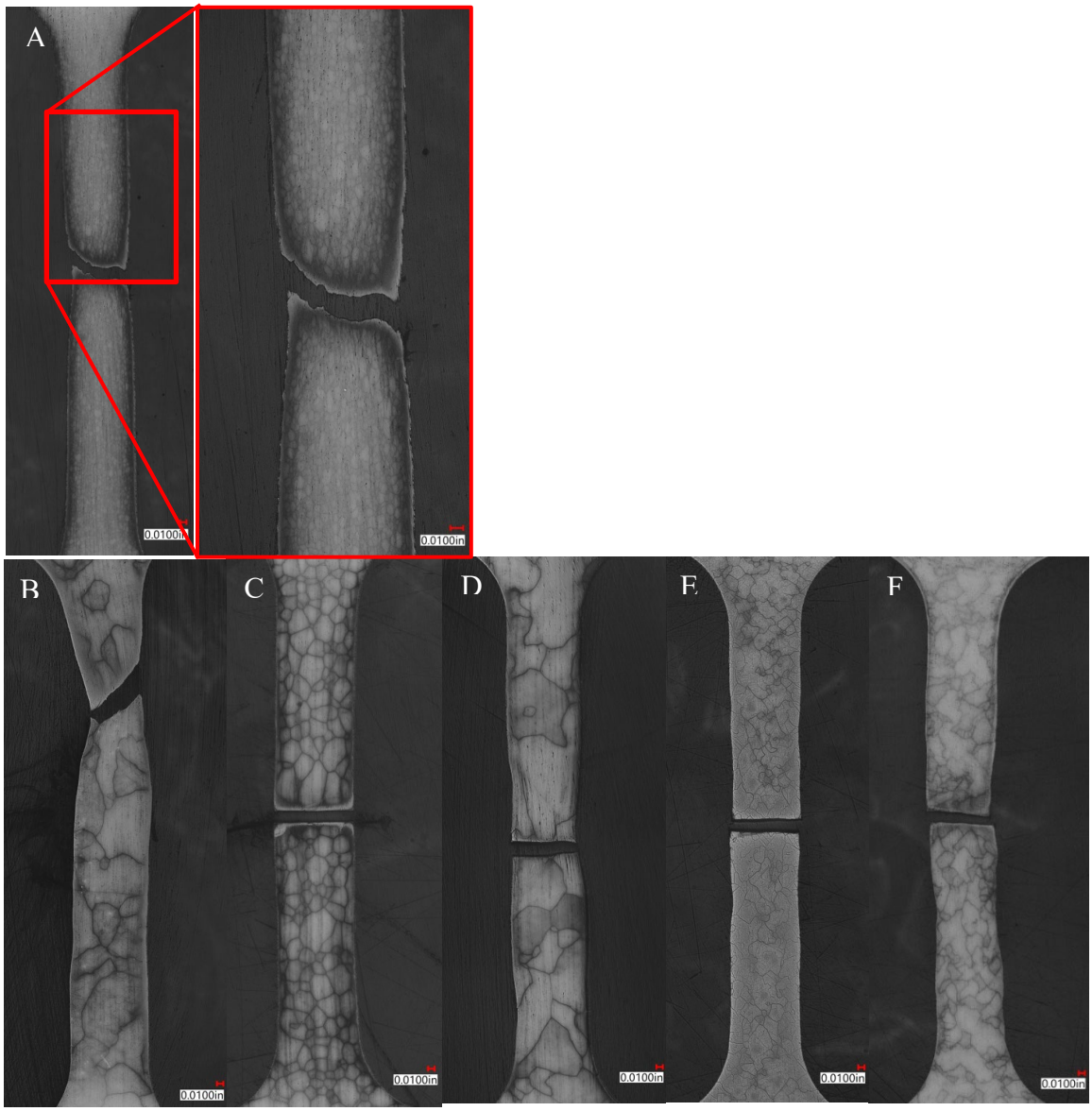

Figure 13: Tensile Sample Metallography of Bonded Joints at 20X Magnification

a. Control sample
b. SN4 (Bonded at 1225°C for 8 hours, RA was<.1µm).
c. SN5 (Bonded at 1225°C for 5 hours, RA was<.14µm).
d. SN6 (Bonded at 1225°C for 4 hours, RA was<.12µm).
e. SN7 (Bonded at 1130°C for 4 hours, RA was<.11µm).
f. SN8 (Bonded at 1175°C for 4 hours, RA was<.11µm).

comparing these results against the stress strain data, it is interesting to infer that strain hardening behavior seemed to be slightly higher than the control sample in SN6 and SN7. This could theoretically indicate that less precipitation occurred in these samples,

supporting the theory that Ostwald Ripening depleted the bulk of precipitation forming elements, due to different strengthening mechanisms affecting the strain hardening behavior. These metallography samples give a clear picture of the amount of grain growth that each parameter set consisted of. It clearly illustrates the correlation between the materials tensile strength is inversely related to the grain size [22].

Fractography was conducted on all samples to evaluate the underlying microstructural causes of fracture. Fracture behavior of the control tensile samples displayed ductile failure in the gauge of the specimen with a sheer lip of approximately 45°. Fracture behavior of bonded samples varied from ductile fracture (in the base material) and brittle fracture at the joint interface. Almost all tensile samples of SN4 and 6 displayed ductile fracture in the base material. SN7 and SN8 had several samples display ductile facture, although most failed in the bond with a brittle type of fracture. Even though SN5 displayed the highest yield strengths of the bonded samples, all tensile tests displayed brittle fracture in the joint interface. This behavior appeared to be a direct result of the grain size, and bond quality. Specifically, the amount of interface closure and the amount of grain crossing contributed to a reduced cross-sectional area at the joint interface due to lack of micro pore closure. Finer grain size assisted the material in achieving higher yield strength. Fractured NbC precipitates were also found in the fracture surface analysis, as shown in Figure 14. All samples, including the base material, displayed the NbC precipitates with fracture going through the precipitate. This indicates that the precipitates

are pinning the grain boundaries and dislocations to some degree and assisting in strain hardening [29]. The size of these precipitates, however, varied dramatically.

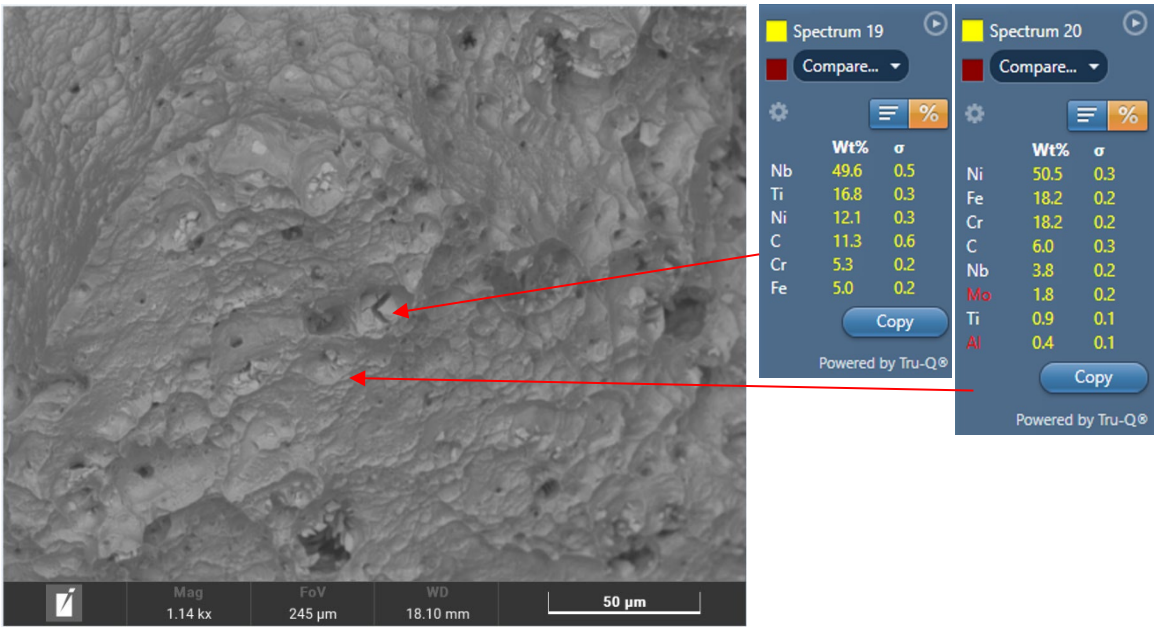

Figure 14: SEM Analysis of Fractured Surface (Sn6)

Hardness test conducted to evaluate the local mechanical properties of the samples showed variations of the hardness due to variation of the parameters. Base material had an average hardness value of 434.81 HV.5. Weldment bonded in hard vacuum (in the precipitation heat treated condition) displayed an average hardness value of 429.72. However, significantly lower values were recorded on samples bonded in argon atmosphere ranging from 376.83 to 408.73. Figure 15, compares each of the sample's average, range of standard deviations of hardness data. All samples displayed significantly higher hardness values in the aged condition than in the as welded condition. Theoretically, this suggests that aging could have caused varying levels of γ" and γ' [26,30]. While the leading theory for the reduced hardness is less precipitation of γ" and γ', due to precipitation forming elements being consumed in large Nb and Ti precipitates via

Ostwald Ripening, large grain sizes can also provide some explanation. The placement of the indentation was random and automated, meaning that samples with smaller grains had a higher likelihood of sampling near a grain boundary, which is known to generally have higher hardness values due to precipitates forming at grain boundaries and increased dislocation densities.

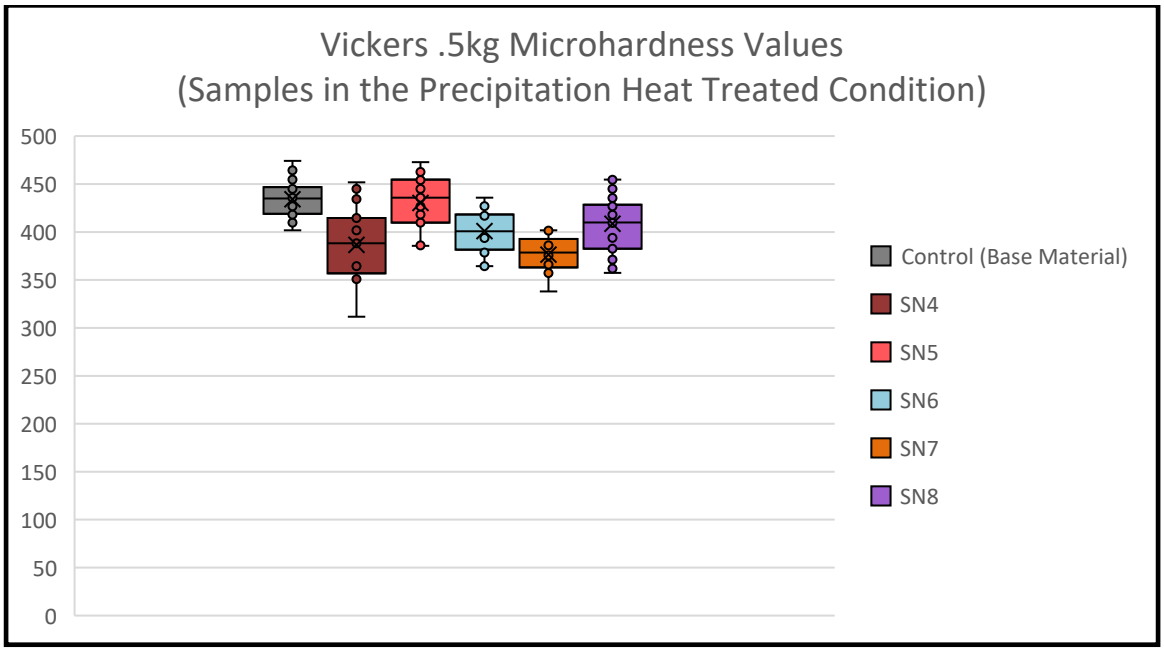

Figure 15: Vickers .5kg Hardness Results of Weldment Population in the Precipitation Heat Treated Condition

4.1 **Conclusions**

Solid state diffusion bonding Inconel 718 to itself at super solvus temperature was studied to establish the effects of the bonding process on the bond formation, grain coalescence and bond's mechanical properties. This information is desired to establish challenges associated with solid state bonding without the aid of an interlayer material.

Literature review showed that bonding at super solvus temperatures would be desired to ensure that detrimental precipitation phases, such as Laves and δ phase, were not formed without the use of elaborate bonding heat treatment cycles. Literature and experimental data showed that maintaining mechanical properties of solid-state diffusion bond depends on stringent controls of the surface finish prior to assembly, reducing the oxide layer present on the faying surfaces of parts, and maintaining a proper balance of achieving volume diffusion while minimizing wide spread grain growth. This research showed that achieving complete coalescence of grains is possible at the expense of refined grain sizes, hence sacrificing the mechanical strength. This increase in grain size decreases the yield and ultimately tensile strength of the material as outlined by Hall-Petch.

Metallurgical testing of all samples showed large Niobium and Titanium rich precipitates linear aligned with the direction of material roll. While these precipitates were observed in all samples, they were significantly smaller in the base material sample. Ostwald Ripening describes the diffusion-controlled growth process of large precipitates at the expense of smaller precipitates. It is hypothesized trough theory and literature review that this phenomenon depleted the crystalline lattice of precipitation forming elements needed to form the strengthening intermetallic phases γ” and γ’.

CHAPTER 5

CONTRIBUTION TO THE SCIENTIFIC COMMUNITY AND INDUSTRY

Sheet Laminate Additive Manufacturing was originally pioneered in the early 1990's and was one of the original additive manufacturing techniques. This technology excels in applications where 3D structures create paths for fluids or gases to flow in strategic manners through a part. Typical applications for this technology are for heat exchangers, fluid valves, microchannel manifolds devices, biomedical implants, nozzles, mixers, and honeycomb seals. Very complex heat exchangers have been manufactured with this technique, which likely could not be manufactured with traditional manufacturing techniques. This technology has largely been underused since it was founded, largely due to the lack of knowledge of its existence, designs lacking applications, high costs associated with tooling, development and relatively low throughput of the diffusion welding process.

The high-quality metallurgical bonds in conjunction with the ability to achieve little to no distortion of the microchannels offered through diffusion bonding and transient liquid phase diffusion bonding open this technology to applications where superior cooling capabilities can be leveraged. With this theory, the technology could be used to advance rotating detonation rocket engines, low altitude hypersonic flight, and fusion reactors since all these applications require extreme design temperatures that our current metal materials are not able to withstand. Other non-metal based applications include some composite based applications such as carbon fiber components, and electrical devices, which would not employ the diffusion bonding process to join laminates.

BIBLIOGRAPHY

1. Lippold, J. C. *Welding Metallurgy and Weldability of Nickel-Base Alloys*. (Wiley, Hoboken, 2009).

2. Kazakov, N. F. Diffusion Bonding of Materials. in *Diffusion Bonding of Materials* 10–16 (Pergamon Press Inc., Maxwell House, Fairview Park, Elmsford, New York 10523, USA, Moscow USSR, 1985). doi:10.1016/B978-0-08-032550-7.50005-9.

3. Maitland, S. C., Hall, P. & Zhou, Y. N. *Welding Handbook, Diffusion Welding and Diffusion Brazing*. vol. 3 Part 2 (The American Welding Society, Miami, Florida, USA).

4. Garrett, B. R., Blank, G. F. & Ranadive, A. J. *BROAD APPLICATIONS OF DIFFUSION BONDING*. https://ntrs.nasa.gov/citations/19660010173 (1966).

5. Paponetti, C. A. & Sapp, M. *Brazing Handbook*. (The American Welding Society, Miami, Florida, USA).

6. Gould, J. E. *et al. Welding Handbook, Other Welding and Cutting Processes*. vol. 3 Part 2 (The American Welding Society, Miami, Florida, USA).

7. Verhoeven, J. Pattern Formation in Wootz Damascus Steel Swords and Blades. *Indian J. Hist. Sci.* **42.4**, 559–574 (2007).

8. Benardos, N. & Olszewski, S. Process of and apparatus for working metals by the direct application of the electric current. (1887).

9. Lincoln, J. *The Procedure Handbook of Arc Welding*. (Cleveland Ohio, 2020).
10. Doherty, R. D. *et al.* Current issues in recrystallization: a review. *Mater. Sci. Eng.* **A238**, 219–274 (1997).

11. Porter, D. A., Easterling, K. E. & Sherif, M. Y. *Phase Transformations in Metal and Alloys*. (2009).

12. Helmut, M. *Diffusion in Solids*. (Springer-Verlag Berlin Heidelberg, University of Munster, 2007).

13. Reed-Hill, R. & Abbaschian, R. *Physical Metallurgy Principles*. (PWS Publishing Company, 1991).

14. Shirzadi, A. A. Diffusion Bonding Aluminium Alloys and Composites: (King's College Cambridge, Cambridge, United Kingdom, 1997).

15. Hill, A. & Wallach, E. R. Modelling Solid-State Diffusion Bodning. *Acta Metall.* **37**, 2425–2437 (1989).

16. Derby, B. & Wallach, E. R. Theoretical Model for Diffusion Bonding. *Met. Sci.* **16**, 49–56 (1982).

17. Ruan, J. J., Ueshima, N. & Oikawa, K. Phase transformations and grain growth behaviors in superalloy 718. *J. Alloys Compd.* **737**, 83–91 (2018).

18. Azadian, S., Wei, L.-Y. & Warren, R. Delta phase precipitation in Inconel 718. *Mater. Charact.* **53**, 7–16 (2004).

19. Thompson, R. G., Dobbs, J. R. & Mayo, D. E. The Effect of Heat Treatment on Microfissuring in Alloy 718. *Weld. J. Res. Suppl.* **65**, (1986).

20. AMS5662: Nickel Alloy, Corrosion- and Heat-Resistant, Bars, Forgings, Rings, and Stock for Forgings and Rings, 52.5Ni - 19Cr - 3.0Mo - 5.1Cb (Nb) - 0.90Ti - 0.50AI - 18Fe, Consumable Electrode or Vacuum Induction Melted, 1775 °F (968 °C) Solution Heat Treated, Precipitation-Hardenable. (2024) doi:10.4271/AMS5662P.

21. Eiselstein, H. L. Age-Hardenable Nickel Alloy (718). (1962).
22. Hall, E. O. The Deformation and Ageing of Mild Steel: III Discussion of Results. *Proc. Phys. Soc. Sect. B* **64**, 747–753 (1951).

23. Guoge, Z., Chandel, R. S., Pheow, S. H. & Hoon, H. H. Effect of Bonding Temperature on the Precipitation of δ Phase in Diffusion Bonded Inconel 718 Joints. *Mater. Manuf. Process.* **21**, 453–457 (2006).

24. Zhang, G., Chandel, R. S. & Seow, H. P. Solid State Diffusion Bonding of Inconel 718. *Sci. Technol. Weld. Join.* **6**, (2001).

25. Pyrometry. (2024) doi:10.4271/AMS2750.

26. Zhang, Y., Lan, L. & Zhao, Y. Effect of precipitated phases on the mechanical properties and fracture mechanisms of Inconel 718 alloy. *Mater. Sci. Eng. A* **864**, 144598 (2023).

27. AMS F Corrosion and Heat Resistant Alloys Committee. Nickel Alloy, Heat Treatment Nickel Alloy and Cobalt Alloy Parts doi:10.4271/AMS2774.

28. E28 Committee. Test Methods for Tension Testing of Metallic Materials. (2024) doi:10.1520/E0008_E0008M-24.

29. Anderson, M., Thielin, A.-L., Bridier, F., Bocher, P. & Savoie, J. δ Phase precipitation in Inconel 718 and associated mechanical properties. *Mater. Sci. Eng. A* **679**, 48–55 (2017).

30. Mignanelli, P. M. *et al.* Gamma-gamma prime-gamma double prime dual-superlattice superalloys. *Scr. Mater.* **136**, 136–140 (2017).

APPENDIX A

FURNACE DATA ACQUSITION LOGS OF DIFFUSION BONDING AND SUBSEQUENT PRECIPITATION HEAT TREATMENT

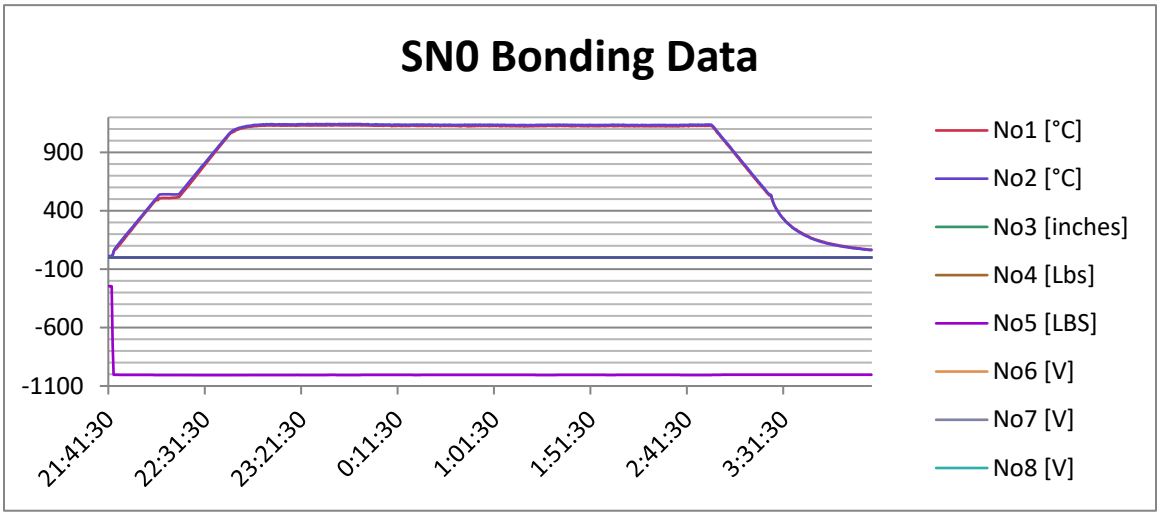
SN0 Bonding Data
900
400
-100
-600
-1100
21:41:30
22:31:30
23:21:30
0:11:30
1:01:30
1:51:30
2:41:30
3:31:30
No1 [°C]
No2 [°C]
No3 [inches]
No4 [Lbs]
No5 [LBS]
No6 [V]
No7 [V]
No8 [V]

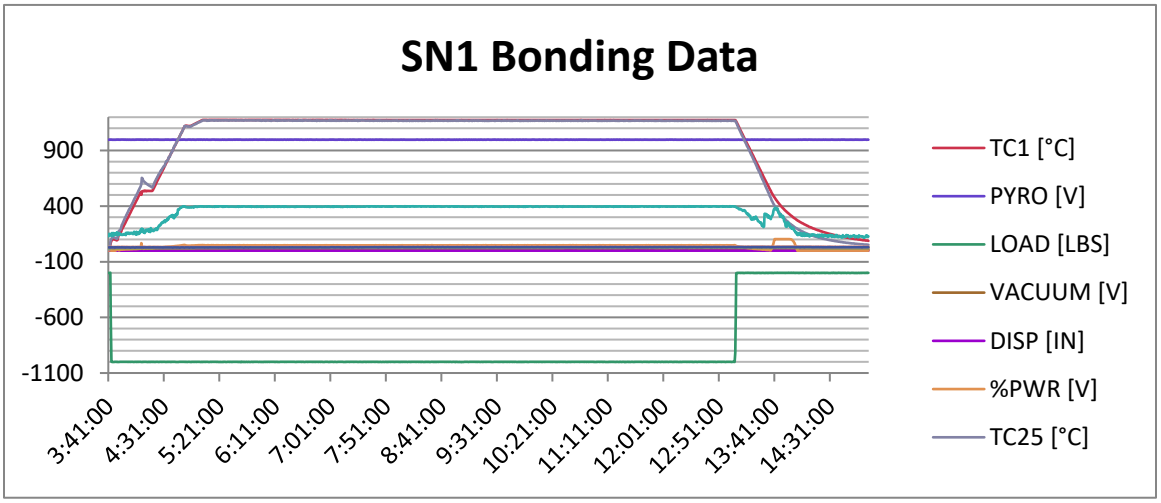
SN1 Bonding Data
900
400
-100
-600
-1100
3:41:00
4:31:00
5:21:00
6:11:00
7:01:00
7:51:00
8:41:00
9:31:00
10:21:00
11:11:00
12:01:00
12:51:00
13:41:00
14:31:00
TC1 [°C]
PYRO [V]
LOAD [LBS]
VACUUM [V]
DISP [IN]
%PWR [V]
TC25 [°C]

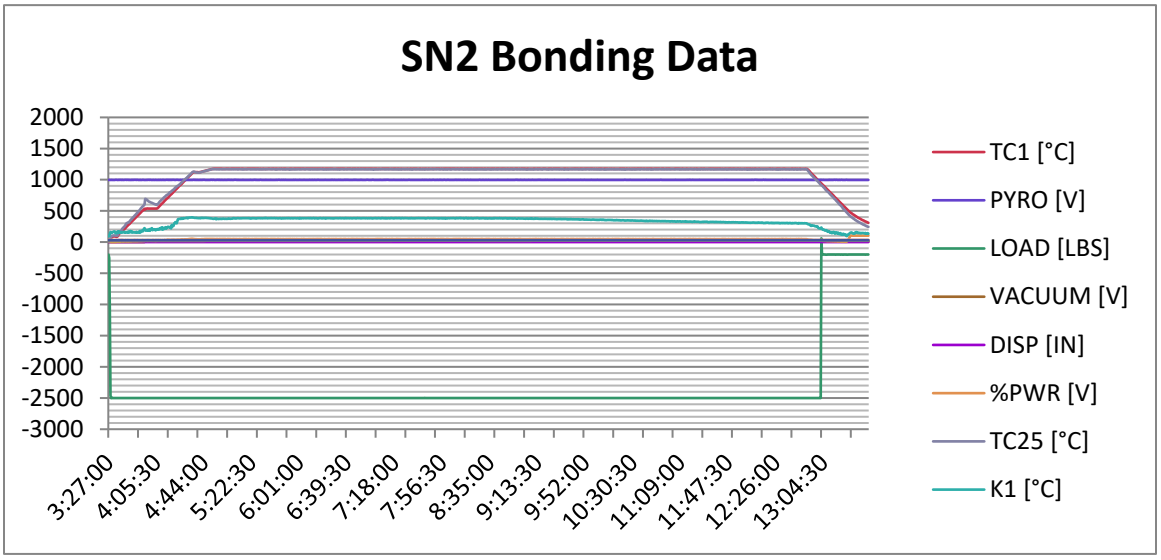
SN2 Bonding Data
2000
1500
1000
500
0
-500
-1000
-1500
-2000
-2500
-3000
3:27:00
4:05:30
4:44:00
5:22:30
6:01:00
6:39:30
7:18:00
7:56:30
8:35:00
9:13:30
9:52:00
10:30:30
11:09:00
11:47:30
12:26:00
13:04:30
TC1 [°C]
PYRO [V]
LOAD [LBS]
VACUUM [V]
DISP [IN]
%PWR [V]
TC25 [°C]
K1 [°C]

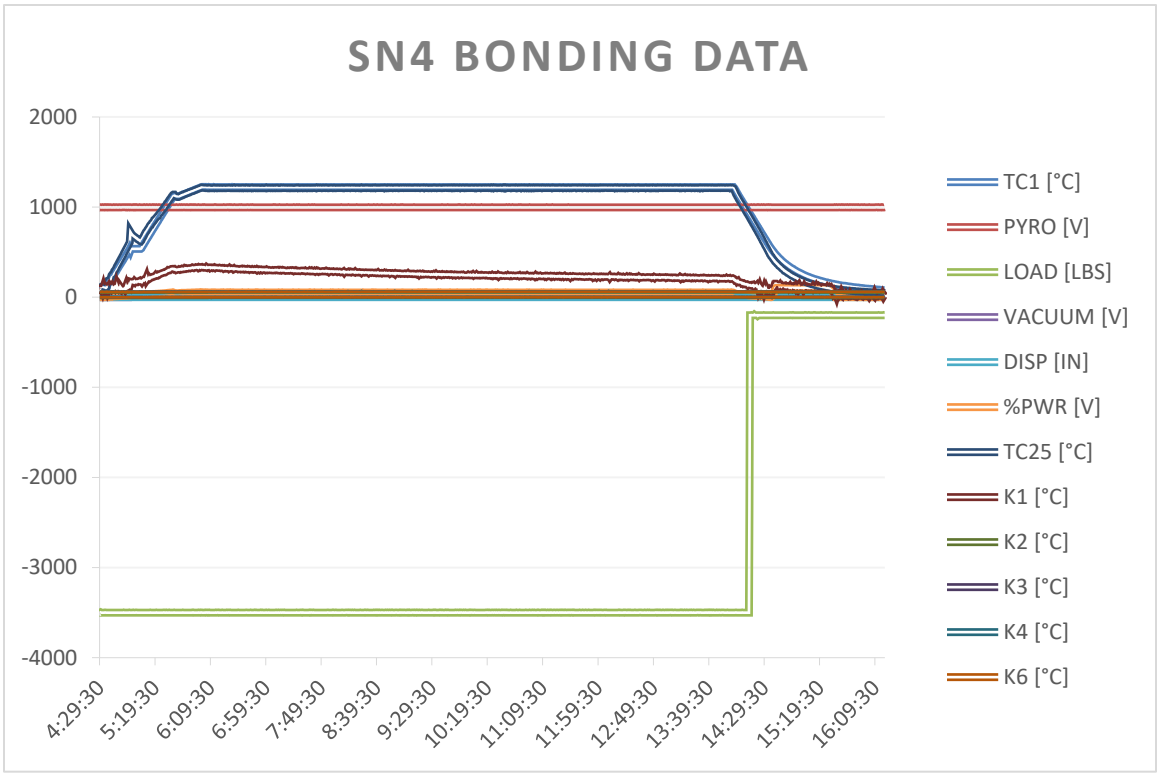
SN4 BONDING DATA
2000
1000
0
-1000
-2000
-3000
-4000
4:29:30
5:19:30
6:09:30
6:59:30
7:49:30
8:39:30
9:29:30
10:19:30
11:09:30
11:59:30
12:49:30
13:39:30
14:29:30
15:19:30
16:09:30
TC1 [°C]
PYRO [V]
LOAD [LBS]
VACUUM [V]
DISP [IN]
%PWR [V]
TC25 [°C]
K1 [°C]
K2 [°C]
K3 [°C]
K4 [°C]
K6 [°C]

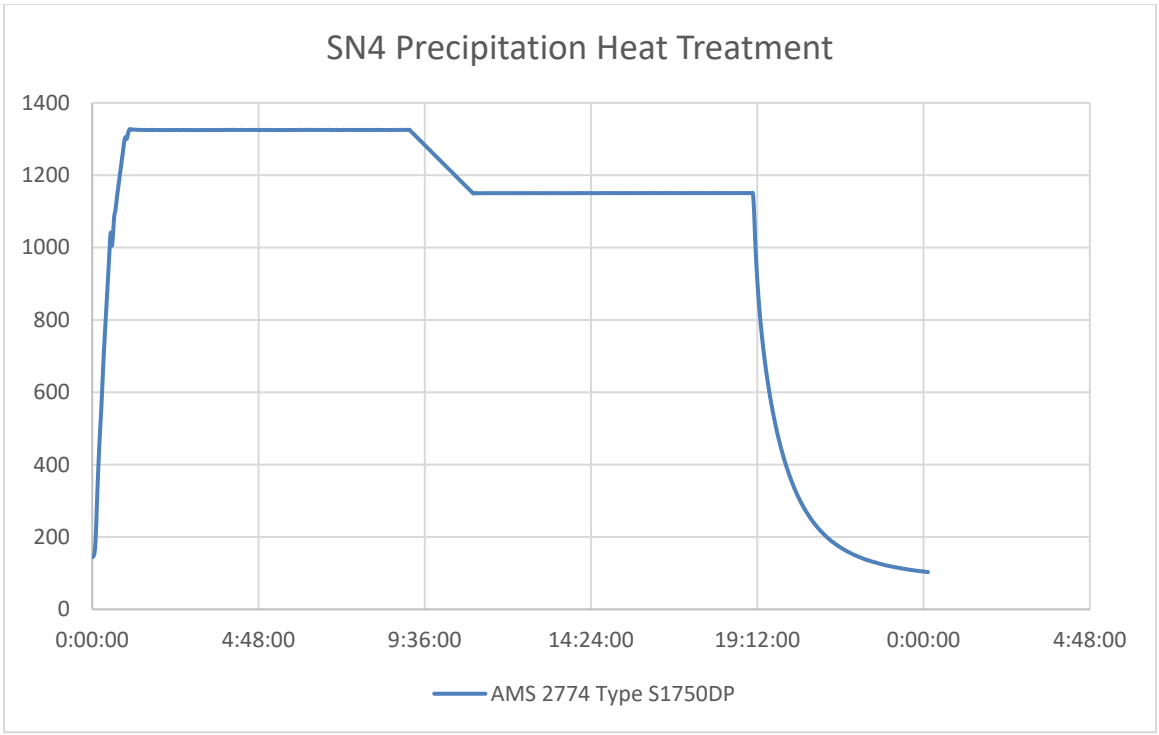
SN4 Precipitation Heat Treatment
1400
1200
1000
800
600
400
200
0
0:00:00
4:48:00
9:36:00
14:24:00
19:12:00
0:00:00
4:48:00
AMS 2774 Type S1750DP

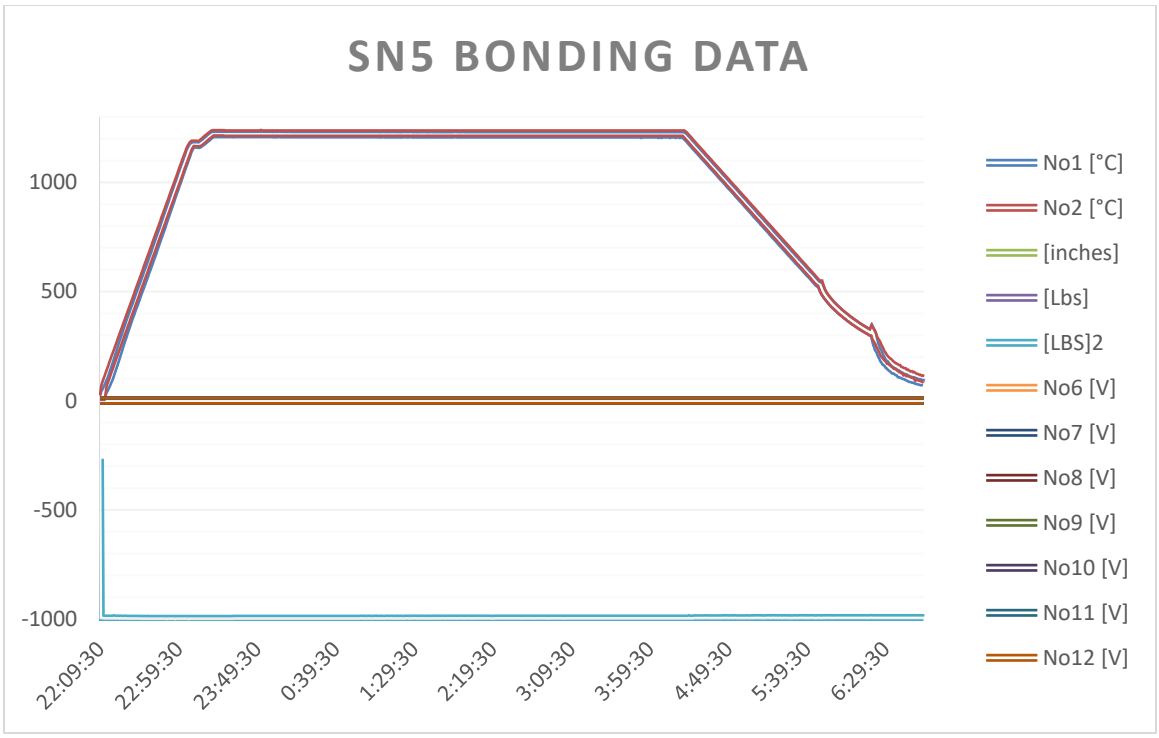
SN5 BONDING DATA
1000
500
0
-500
-1000
22:09:30
22:59:30
23:49:30
0:39:30
1:29:30
2:19:30
3:09:30
3:59:30
4:49:30
5:39:30
6:29:30
No1 [°C]
No2 [°C]
[inches]
[Lbs]
[LBS]2
No6 [V]
No7 [V]
No8 [V]
No9 [V]
No10 [V]
No11 [V]
No12 [V]

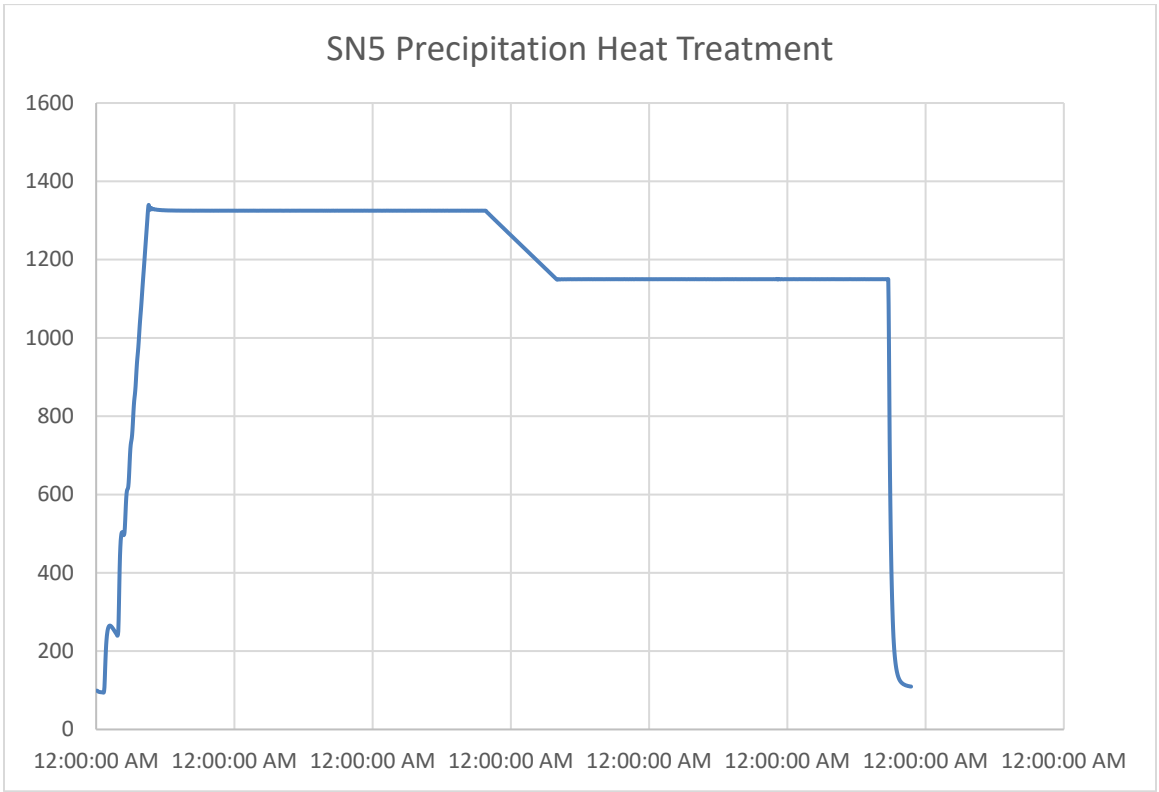
SN5 Precipitation Heat Treatment
1600
1400
1200
1000
800
600
400
200
0
12:00:00 AM
12:00:00 AM
12:00:00 AM
12:00:00 AM
12:00:00 AM
12:00:00 AM
12:00:00 AM
12:00:00 AM

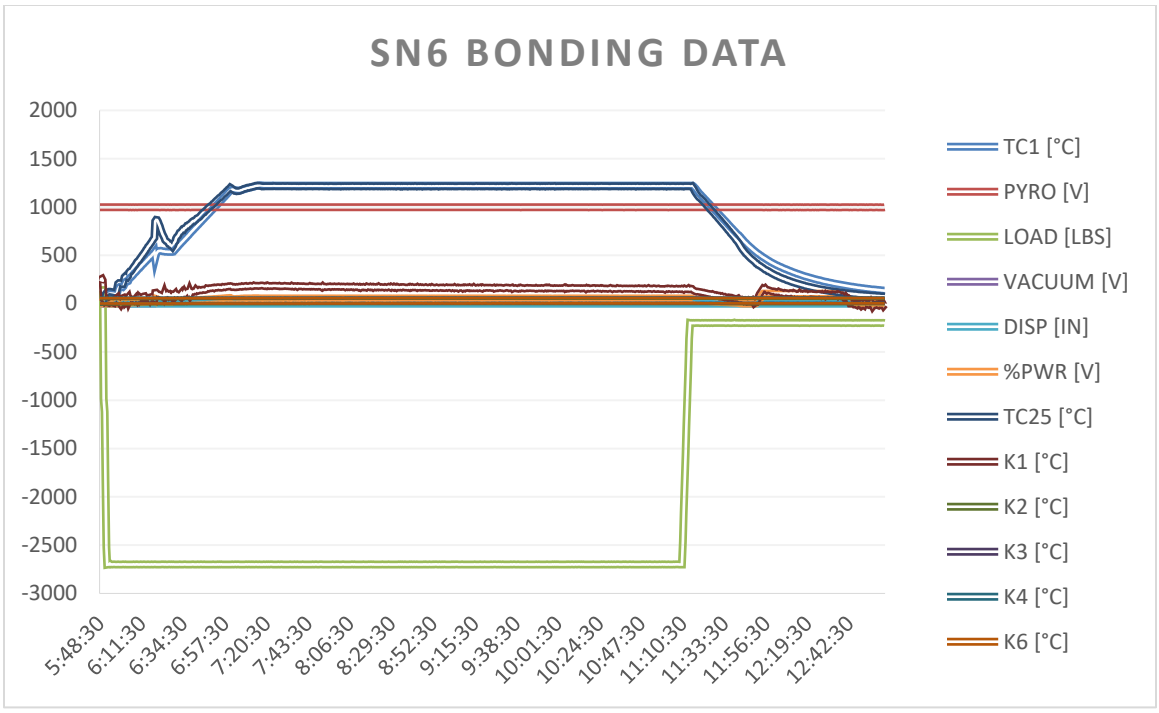
SN6 BONDING DATA
2000
1500
1000
500
0
-500
-1000
-1500
-2000
-2500
-3000
5:48:30
6:11:30
6:34:30
6:57:30
7:20:30
7:43:30
8:06:30
8:29:30
8:52:30
9:15:30
9:38:30
10:01:30
10:24:30
10:47:30
11:10:30
11:33:30
11:56:30
12:19:30
12:42:30
TC1 [°C]
PYRO [V]
LOAD [LBS]
VACUUM [V]
DISP [IN]
%PWR [V]
TC25 [°C]
K1 [°C]
K2 [°C]
K3 [°C]
K4 [°C]
K6 [°C]

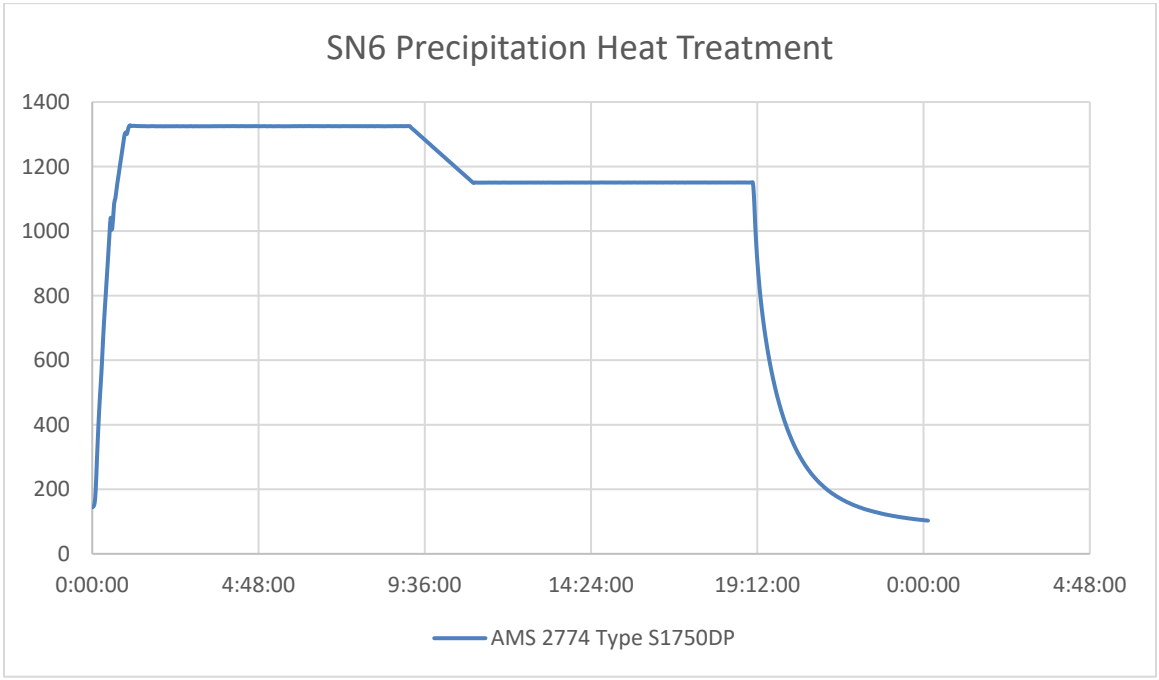
SN6 Precipitation Heat Treatment
1400
1200
1000
800
600
400
200
0
0:00:00
4:48:00
9:36:00
14:24:00
19:12:00
0:00:00
4:48:00
AMS 2774 Type S1750DP

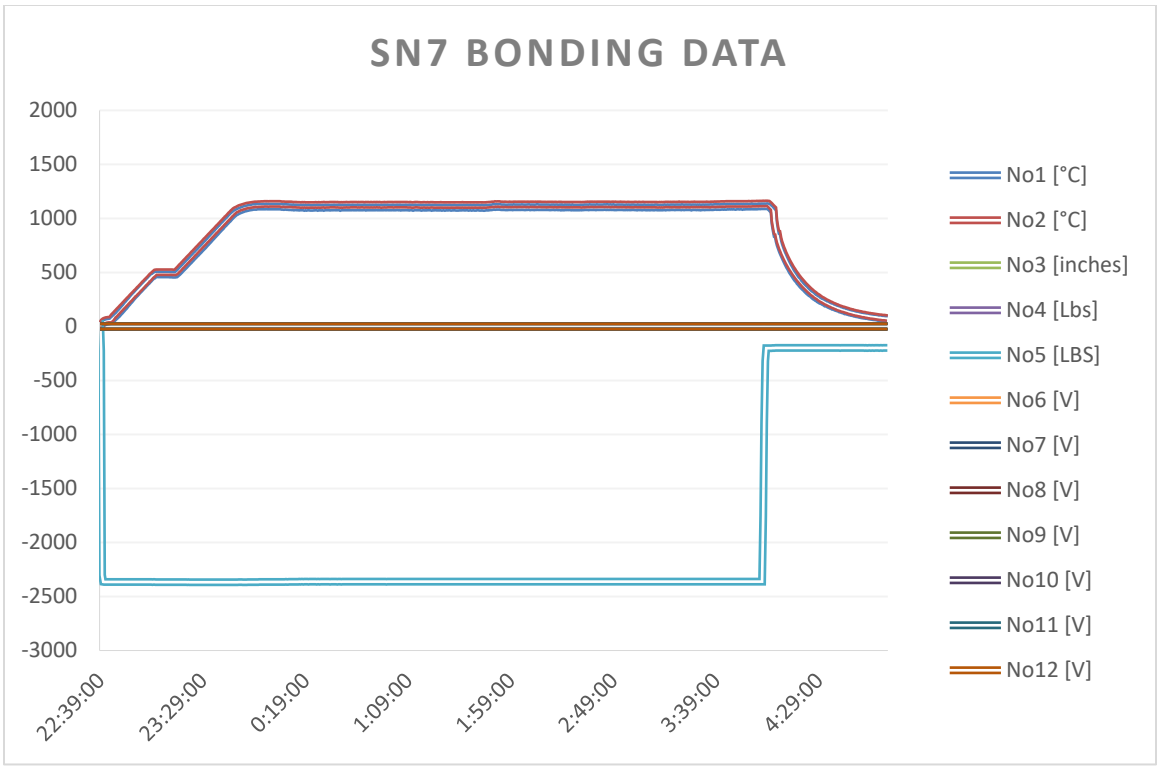
SN7 BONDING DATA
2000
1500
1000
500
0
-500
-1000
-1500
-2000
-2500
-3000
22:39:00
23:29:00
0:19:00
1:09:00
1:59:00
2:49:00
3:39:00
4:29:00
No1 [°C]
No2 [°C]
No3 [inches]
No4 [Lbs]
No5 [LBS]
No6 [V]
No7 [V]
No8 [V]
No9 [V]
No10 [V]
No11 [V]
No12 [V]

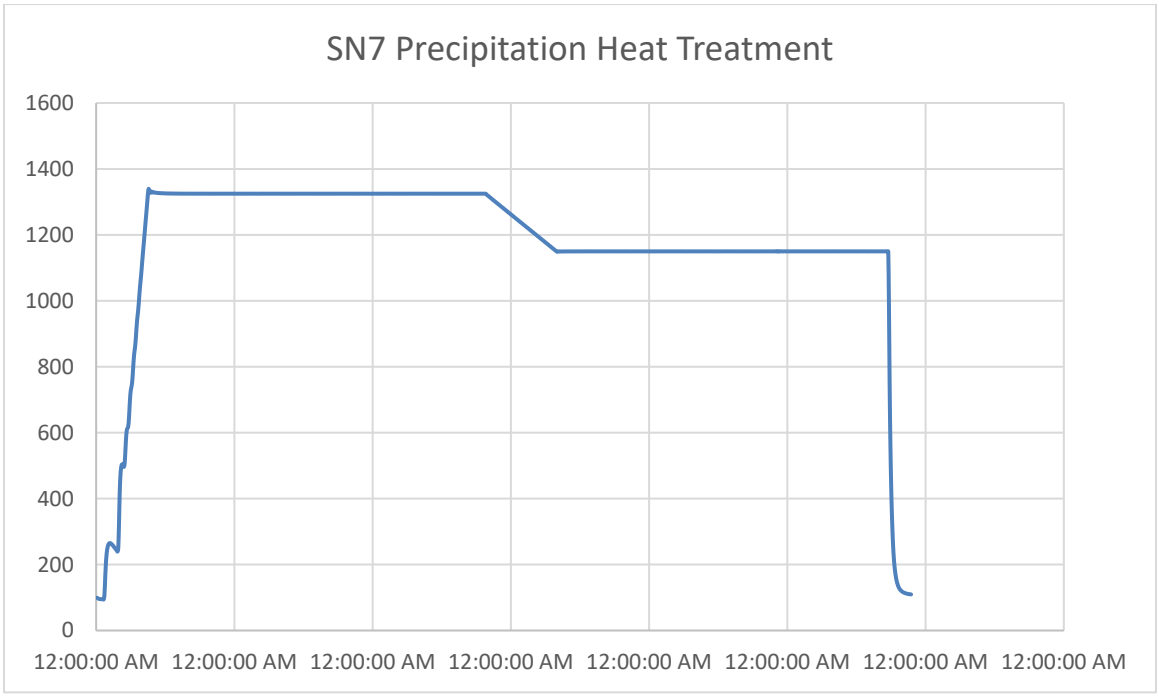
SN7 Precipitation Heat Treatment
1600
1400
1200
1000
800
600
400
200
0
12:00:00 AM
12:00:00 AM
12:00:00 AM
12:00:00 AM
12:00:00 AM
12:00:00 AM
12:00:00 AM
12:00:00 AM

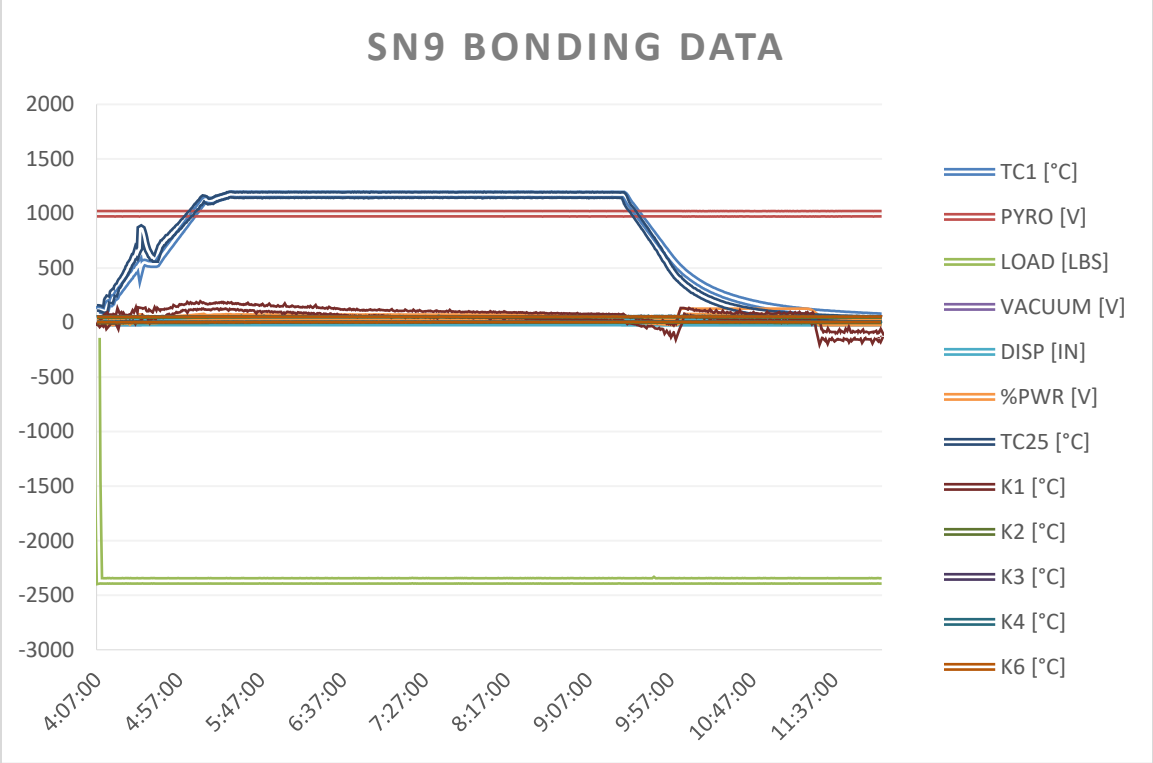
SN9 BONDING DATA
2000
1500
1000
500
0
-500
-1000
-1500
-2000
-2500
-3000
4:07:00
4:57:00
5:47:00
6:37:00
7:27:00
8:17:00
9:07:00
9:57:00
10:47:00
11:37:00
TC1 [°C]
PYRO [V]
LOAD [LBS]
VACUUM [V]
DISP [IN]
%PWR [V]
TC25 [°C]
K1 [°C]
K2 [°C]
K3 [°C]
K4 [°C]
K6 [°C]

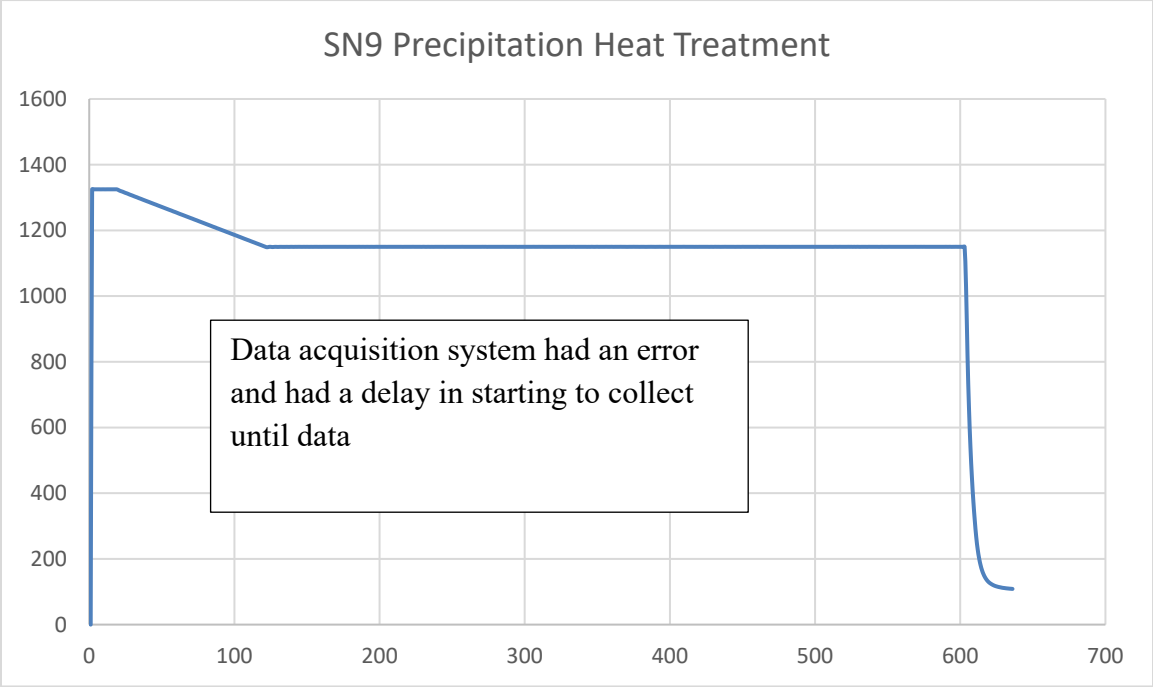
SN9 Precipitation Heat Treatment
1600
1400
1200
1000
800
600
400
200
0
0
100
200
300
400
500
600
700
Data acquisition system had an error and had a delay in starting to collect until data

APPENDIX B

TENSIL TESTING DATA COLLECTED FROM SAMPLE POPULATION

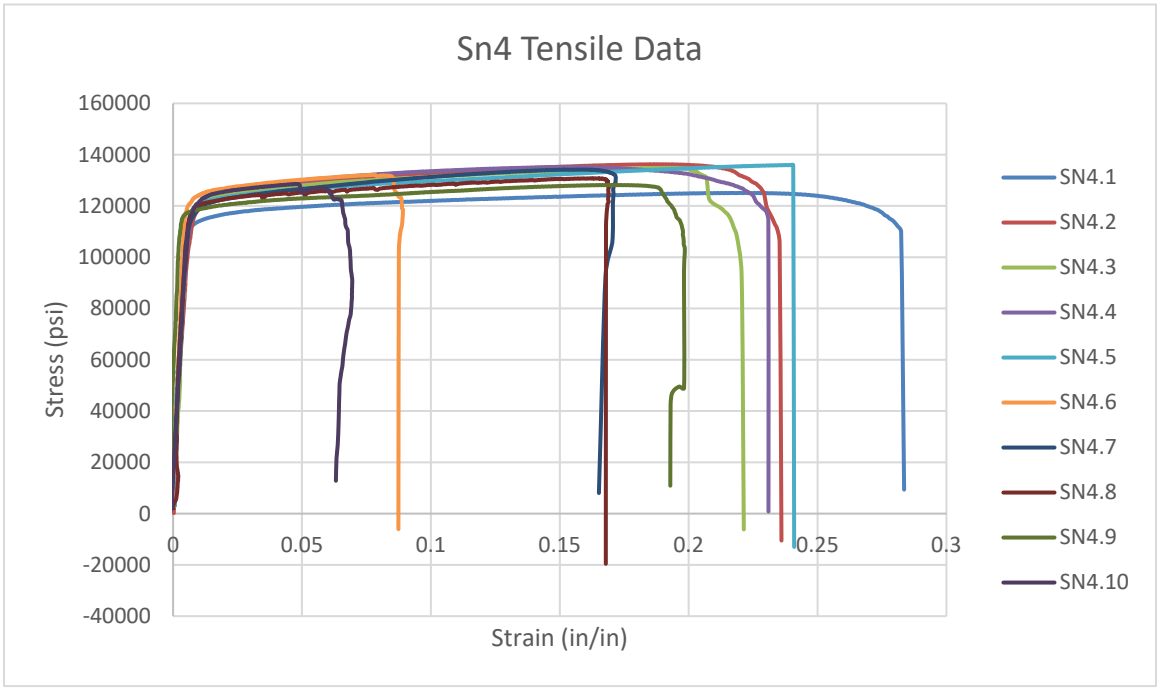
Sn4 Tensile Data
160000
140000
120000
100000
80000
60000
40000
20000
0
-20000
-40000
Stress (psi)
0
0.05
0.1
0.15
0.2
0.25
0.3
Strain (in/in)
SN4.1
SN4.2
SN4.3
SN4.4
SN4.5
SN4.6
SN4.7
SN4.8
SN4.9
SN4.10

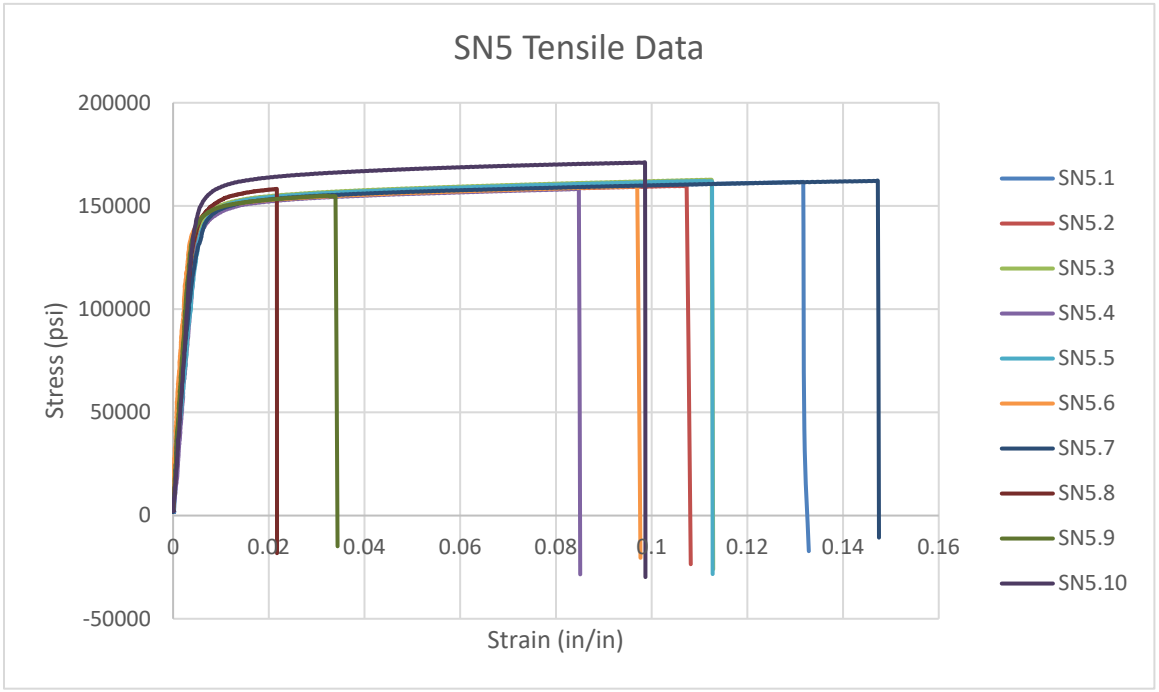
SN5 Tensile Data
200000
150000
100000
50000
0
-50000
Stress (psi)
0
0.02
0.04
0.06
0.08
0.1
0.12
0.14
0.16
Strain (in/in)
SN5.1
SN5.2
SN5.3
SN5.4
SN5.5
SN5.6
SN5.7
SN5.8
SN5.9
SN5.10

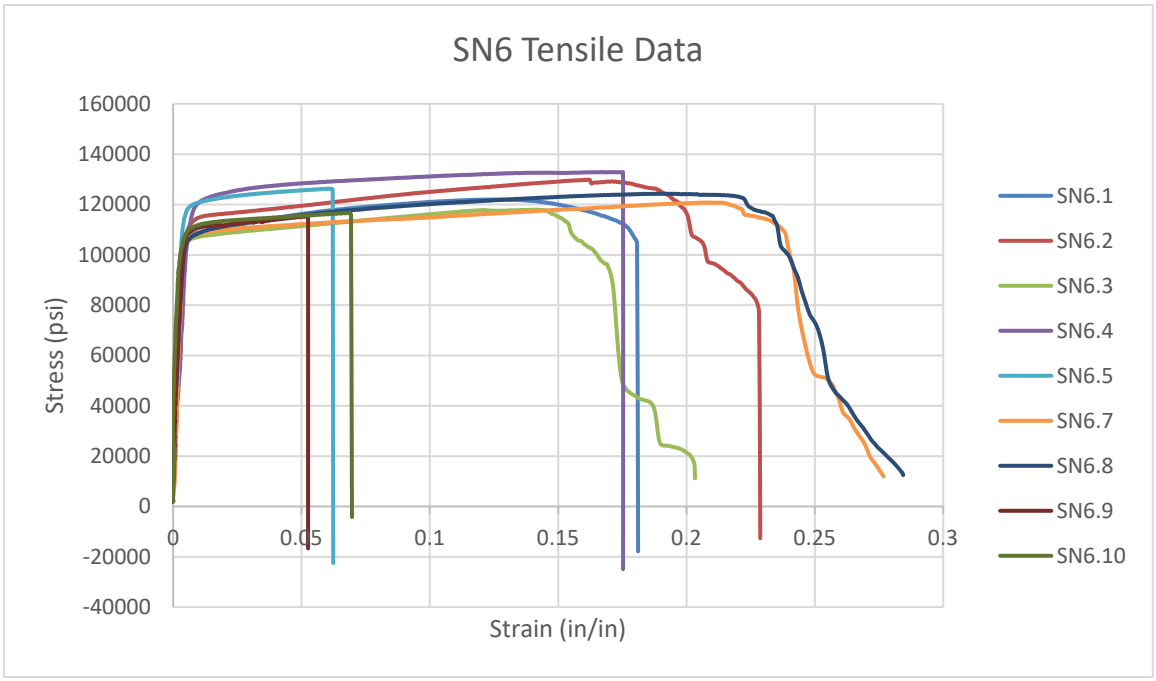
SN6 Tensile Data
160000
140000
120000
100000
80000
60000
40000
20000
0
-20000
-40000
Stress (psi)
0
0.05
0.1
0.15
0.2
0.25
0.3
Strain (in/in)
SN6.1
SN6.2
SN6.3
SN6.4
SN6.5
SN6.7
SN6.8
SN6.9
SN6.10

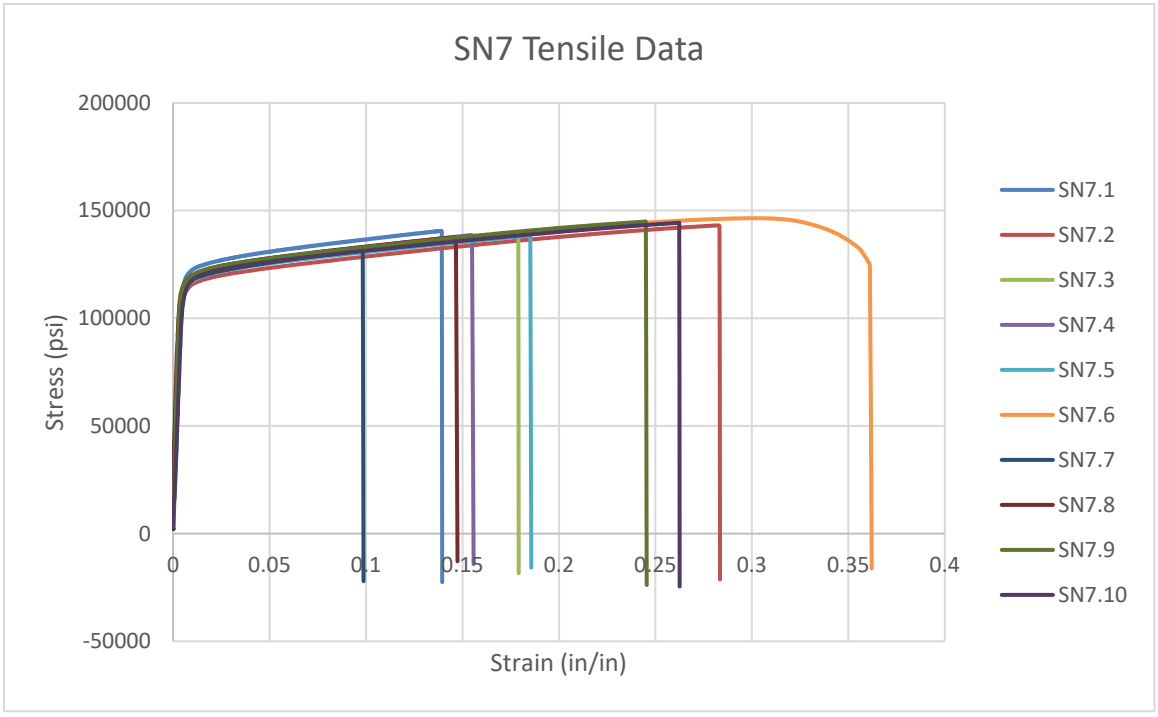
SN7 Tensile Data
200000
150000
100000
50000
0
-50000
Stress (psi)
0
0.05
0.1
0.15
0.2
0.25
0.3
0.35
0.4
Strain (in/in)
SN7.1
SN7.2
SN7.3
SN7.4
SN7.5
SN7.6
SN7.7
SN7.8
SN7.9
SN7.10

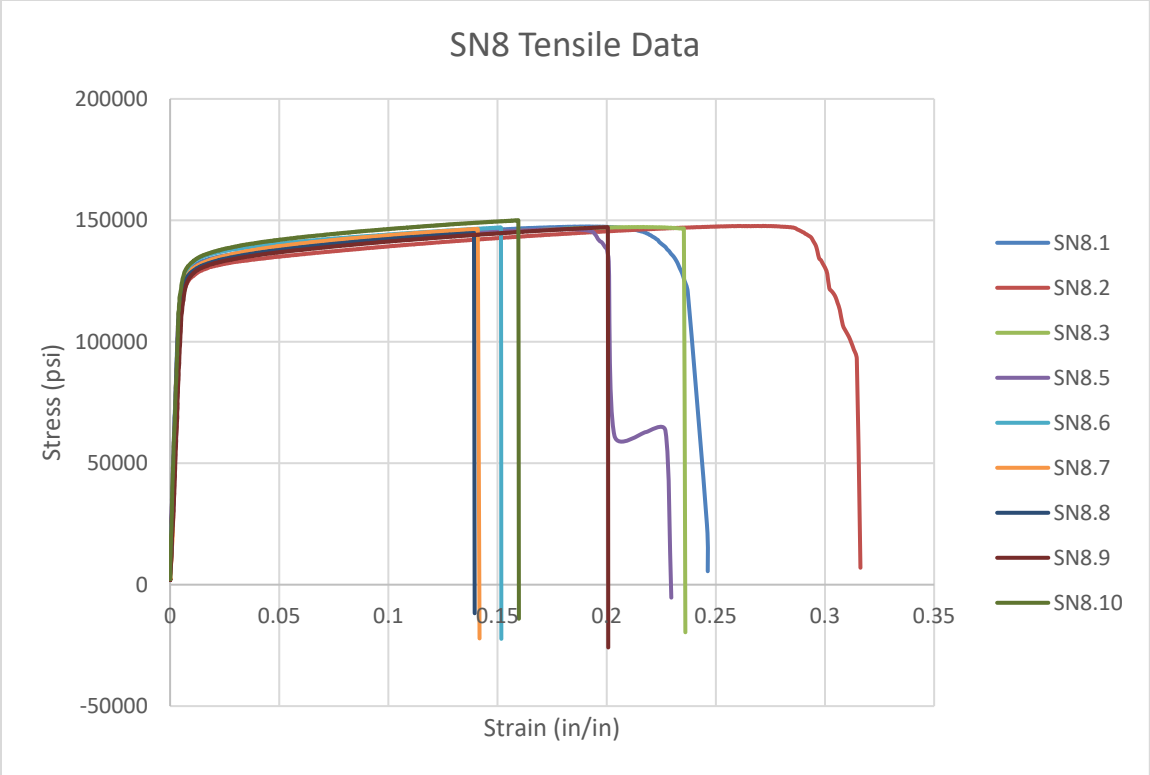
SN8 Tensile Data
200000
150000
100000
50000
0
-50000
Stress (psi)
0
0.05
0.1
0.15
0.2
0.25
0.3
0.35
Strain (in/in)
SN8.1
SN8.2
SN8.3
SN8.5
SN8.6
SN8.7
SN8.8
SN8.9
SN8.10